

Long-term thermal sensitivity of Earth's tropical forests

Martin J. P. Sullivan^{1,2}, Simon L. Lewis^{1,3}, Kofi Affum-Baffoe⁴, Carolina Castilho⁵, Flávia Costa⁶, Aida Cuni Sanchez^{7,8}, Corneille E. N. Ewango^{9,10,11}, Wannos Hubau^{1,12,13}, Beatriz Marimon¹⁴, Abel Monteagudo-Mendoza¹⁵, Lan Qie¹⁶, Bonaventure Sonké¹⁷, Rodolfo Vasquez Martinez¹⁵, Timothy R Baker¹, Roel J. W. Brienen¹, Ted R. Feldpausch¹⁸, David Galbraith¹, Manuel Gloor¹, Yadvinder Malhi¹⁹, Shin-Ichiro Aiba²⁰, Miguel N. Alexiades²¹, Everton C. Almeida²², Edmar Almeida de Oliveira²³, Esteban Álvarez Dávila²⁴, Patricia Alvarez Loayza²⁵, Ana Andrade²⁶, Simone Aparecida Vieira²⁷, Luiz Aragão²⁸, Alejandro Araujo-Murakami²⁹, Eric J.M.M. Arets³⁰, Luzmila Arroyo³¹, Peter Ashton³², Gerardo Aymard C.³³, Fabrício B. Baccaro³⁴, Lindsay F. Banin³⁵, Christopher Baraloto³⁶, Plínio Barbosa Camargo³⁷, Jos Barlow³⁸, Jorcely Barroso³⁹, Jean-François Bastin⁴⁰, Sarah A. Batterman^{1,41,42,43}, Hans Beeckman¹², Serge K. Begne^{17,44}, Amy C. Bennett⁴⁴, Erika Berenguer^{19,38}, Nicholas Berry⁴⁵, Lilian Blanc⁴⁶, Pascal Boeckx⁴⁷, Jan Bogaert⁴⁸, Damien Bonal⁴⁹, Frans Bongers⁵⁰, Matt Bradford⁵¹, Francis Q. Brearley², Terry Brncic⁵², Foster Brown⁵³, Benoit Burban⁵⁴, José Luís Camargo²⁶, Wendeson Castro⁵⁵, Carlos Céron⁵⁶, Sabina Cerruto Ribeiro⁵⁷, Victor Chama Moscoso¹⁵, Jérôme Chave⁵⁸, Eric Chezeaux⁵⁹, Connie J. Clark²⁵, Fernanda Coelho¹, Murray Collins⁶¹, James A. Comiskey^{62,63}, Fernando Cornejo Valverde⁶⁴, Massiel Corrales Medina⁶⁵, Lola da Costa⁶⁶, Martin Dančák⁶⁷, Greta C. Dargie¹, Stuart Davies⁶⁸, Nallaret Davila Cardozo⁶⁹, Thales de Haulleville^{12,48}, Marcelo Brillhante de Medeiros⁷⁰, Jhon del Aguila Pasquel⁷¹, Géraldine Derroire⁷², Anthony Di Fiore⁷³, Jean-Louis Doucet⁷⁴, Aurélie Dourdain⁷², Vincent Droissant⁷⁵, Luisa Fernanda Duque⁷⁶, Romeo Ekoungoulou⁷⁷, Fernando Elias⁷⁸, Terry Erwin⁷⁹, Adriane Esquivel-Muelbert⁸⁰, Sophie Fauset⁸¹, Joice Ferreira⁸², Gerardo Flores Llampazo⁸³, Ernest Foli⁸⁴, Andrew Ford⁵¹, Martin Gilpin¹, Jefferson S. Hall⁸⁵, Keith C. Hamer⁸⁶, Alan C. Hamilton⁸⁷, David J. Harris⁸⁸, Terese B. Hart^{89,90}, Radim Hédli^{91,92}, Bruno Herault⁷², Rafael Herrera⁹³, Niro Higuchi⁶, Annette Hladik⁹⁴, Eurídice Honorio Coronado⁷¹, Isau Huamantupa-Chuquimaco⁹⁵, Walter Huaraca Huasco⁹⁵, Kathryn J. Jeffery⁹⁶, Eliana Jimenez-Rojas⁹⁷, Michelle Kalamandeen¹, Marie-Noel Kamdem^{11,13,17,98}, Elizabeth Kearsley⁹⁹, Ricardo Keichi Umetsu¹⁰⁰, Lip Khoon Kho¹⁰¹, Timothy Killeen¹⁰², Kanehiro Kitayama¹⁰³, Bente Klitgaard¹⁰⁴, Alexander Koch¹⁰⁵, Nicolas Labrière⁵⁸, William Laurance¹⁰⁶, Susan Laurance¹⁰⁶, Miguel E. Leal¹⁰⁷, Aurora Levesley¹, Adriano J. N. Lima⁶, Janvier Lisingo¹¹, Aline P. Lopes^{108,109}, Gabriela Lopez-Gonzalez¹, Tom Lovejoy¹¹⁰, Jon Lovett¹, Richard Lowe¹¹¹, William E. Magnusson¹¹², Jagoba Malumbres-Olarte^{113,114}, Ângelo Gilberto Manzatto¹¹⁵, Ben Hur Marimon Junior¹¹⁶, Andrew R. Marshall^{8,117,118}, Toby Marthews¹¹⁹, Simone Matias de Almeida Reis^{14,19}, Colin Maycock¹²⁰, Karina Melgaço¹, Casimiro Mendoza¹²¹, Faizah Metali¹²², Vianet Mihindou^{123,124}, William Milliken¹⁰⁴, Edward Mitchard¹²⁵, Paulo S. Morandi¹⁴, Hannah L. Mossman², Laszlo Nagy¹²⁶, Henrique Nascimento⁶, David Neill¹²⁷, Reuben Nilus¹²⁸, Percy Núñez Vargas⁹⁵, Walter Palacios¹²⁹, Nadir Pallqui Camacho^{1,95}, Julie Peacock¹, Colin Pendry¹³⁰, Maria Cristina Peñuela Mora¹³¹, Georgia C. Pickavance¹, John Pipoly¹³², Nigel Pitman¹³³, Maureen Playfair¹³⁴, Lourens Poorter¹³⁵, John R. Poulsen²⁵, Axel D. Poulsen¹³⁶, Richard Preziosi², Adriana Prieto¹³⁷, Richard Primack¹³⁸, Hirma Ramírez-Angulo¹³⁹, Jan Reitsma¹⁴⁰, Maxime Réjou-Méchain⁷⁵, Zorayda Restrepo Correa¹⁴¹, Thaianne Rodrigues de Sousa⁶, Lily Rodriguez Bayona¹⁴², Anand Roopsind¹⁴³, Agustín Rudas¹³⁷, Ervan Rutishauser^{42,144}, Kamariah Abu Salim¹²², Rafael P. Salomão^{145,146}, Juliana Schiatti⁶, Douglas Sheil¹⁴⁷, Richarly C. Silva^{57,148}, Javier Silva Espejo¹⁴⁹, Camila Silva Valeria³⁸, Marcos Silveira⁵⁷, Murielle Simo-Droissart¹⁷, Marcelo Fragomeni Simon⁷⁰, James Singh¹⁵⁰, Yahn Carlos Soto Shareva¹⁵, Clement Stahl⁵⁴, Juliana Stropp¹⁵¹, Rahayu Sukri¹²², Terry Sunderland^{152,153}, Martin Svátek¹⁵⁴, Michael D. Swaine¹⁵⁵, Varun Swamy¹⁵⁶, Hermann Taedoung¹⁷, Joey Talbot¹, James Taplin¹⁵⁷, David Taylor¹⁵⁸, Hans ter Steege^{159,160}, John Terborgh²⁵, Raquel Thomas¹⁴³, Sean C. Thomas¹⁶¹, Armando Torres-Lezama¹⁶², Peter Umunay^{163,164}, Luis Valenzuela Gamarra¹⁵, Geertje van der Heijden¹⁶⁵, Peter van der Hout¹⁶⁶, Peter van der Meer¹⁶⁷, Mark van Nieuwstadt¹⁶⁸, Hans Verbeeck⁹⁹, Ronald Vernimmen¹⁶⁹, Alberto Vicentini⁶, Ima Célia Guimarães Vieira¹⁴⁶, Emilio Vilanova Torre¹⁷⁰, Jason Vleminckx³⁶, Vincent Vos¹⁷², Ophelia Wang¹⁷³, Lee J. T. White^{124,174,175}, Simon Willcock¹⁷⁶, John T. Woods¹⁷⁷, Verginia Wortel¹⁷⁸, Kenneth Young¹⁷⁹, Roderick Zagt¹⁸⁰, Lise Zemagho¹⁷, Pieter A. Zuidema⁵⁰, Joeri A. Zwarts^{178,181}, Oliver L. Phillips¹

Affiliations:

- 1 School of Geography, University of Leeds, Leeds, UK
- 2 Department of Natural Sciences, Manchester Metropolitan University, Manchester, UK
- 3 Department of Geography, University College London, London, UK
- 4 Mensuration Unit, Forestry Commission of Ghana, Kumasi, Ghana
- 5 Embrapa Roraima, Brazilian Agricultural Research Corporation (EMBRAPA), Brasília, Brazil
- 6 Instituto Nacional de Pesquisas da Amazônia (INPA), Manaus, Brazil
- 7 Department of Ecosystem Science and Sustainability, Colorado State University, USA
- 8 Department of Environment and Geography, University of York, York, UK
- 9 DR Congo Programme, Wildlife Conservation Society, Kisangani, Democratic Republic of Congo
- 10 Centre de Formation et de Recherche en Conservation Forestiere (CEFRECOF), Epulu, Democratic Republic of Congo
- 11 Faculté de Gestion de Ressources Naturelles Renouvelables, Université de Kisangani, Kisangani, Democratic Republic of Congo
- 12 Service of Wood Biology, Royal Museum for Central Africa, Tervuren, Belgium
- 13 Department of Environment, Laboratory of Wood Technology (Woodlab), Ghent University, Ghent, Belgium
- 14 Faculdade de Ciências Agrárias, Biológicas e Sociais Aplicadas, Universidade do Estado de Mato Grosso, Nova Xavantina-MT, Brazil
- 15 Jardín Botánico de Missouri, Oxapampa, Peru
- 16 School of Life Sciences, University of Lincoln, Lincoln, UK
- 17 Plant Systematics and Ecology Laboratory, Higher Teachers' Training College, University of Yaoundé I, Yaoundé, Cameroon
- 18 Geography, College of Life and Environmental Sciences, University of Exeter, Exeter, UK
- 19 Environmental Change Institute, School of Geography and the Environment, University of Oxford, Oxford, UK
- 20 Graduate School of Science and Engineering, Kagoshima University, Japan
- 21 School of Anthropology and Conservation, University of Kent, Canterbury, UK
- 22 Instituto de Biodiversidade e Florestas, Universidade Federal do Oeste do Pará, Santarém - PA, Brazil
- 23 Universidade do Estado de Mato Grosso, Cáceres - MT, Brazil
- 24 Escuela de Ciencias Agrícolas, Pecuarias y del Medio Ambiente, National Open University and Distance, Colombia
- 25 Center for Tropical Conservation, Nicholas School of the Environment, Duke University, Durham, NC, USA
- 26 Projeto Dinâmica Biológica de Fragmentos Florestais, Instituto Nacional de Pesquisas da Amazônia, Manaus, Brazil
- 27 Universidade Estadual de Campinas, Campinas - SP, Brazil
- 28 National Institute for Space Research (INPE), São José dos Campos-SP, Brazil
- 29 Museo de Historia Natural Noel Kempff Mercado, Universidad Autónoma Gabriel René Moreno, Santa Cruz, Bolivia
- 30 Wageningen Environmental Research, Wageningen, The Netherlands
- 31 Dirección de la Carrera de Biología, Universidad Autónoma Gabriel René Moreno, Santa Cruz, Bolivia
- 32 Department of Organismic and Evolutionary Biology, Harvard University, Cambridge, MA, USA
- 33 Programa de Ciencias del Agro y el Mar, Herbario Universitario, Barinas, Venezuela
- 34 Departamento de Biologia, Universidade Federal do Amazonas, Manaus, Brazil

- 35 Centre of Ecology and Hydrology, Penicuik, UK
- 36 International Center for Tropical Botany, Department of Biological Sciences, Florida International
University, Florida, FL, USA
- 37 Centro de Energia Nuclear na Agricultura, Universidade de São Paulo, São Paulo, SP, Brazil
- 38 Lancaster Environment Centre, Lancaster University, Lancaster, UK
- 39 Centro Multidisciplinar, Universidade Federal do Acre, Cruzeiro do Sul - AC, Brazil
- 40 Institute of Integrative Biology, ETH Zurich, Zurich, Switzerland
- 41 Priestley International Centre for Climate, University of Leeds, Leeds, UK
- 42 Smithsonian Tropical Research Institute, Panama, Panama
- 43 Cary Institute of Ecosystem Studies, Millbrook, NY, USA
- 44 School of Geography, School of Geography, Leeds, UK
- 45 The Landscapes and Livelihoods Group, Edinburgh, UK
- 46 UR Forest & Societies, CIRAD, Montpellier, France
- 47 Isotope Bioscience Laboratory-ISOFYS, Ghent University, Ghent, Belgium
- 48 Gembloux Agro-Bio Tech, University of Liège, Liège, Belgium
- 49 UMR Silva, INRA, Nancy, France
- 50 Department of Forest Ecology and Forest Management Group, Wageningen University, Wageningen,
The Netherlands
- 51 CSIRO, Canberra, Australia
- 52 Congo Programme, Wildlife Conservation Society, Brazzaville, Republic of Congo
- 53 Woods Hole Research Center, Falmouth, MA, USA
- 54 Ecologie des Forêts de Guyane (ECOFOG), INRA, Kourou, French Guiana
- 55 Programa de Pós-Graduação Ecologia e Manejo de Recursos Naturais, Universidade Federal do Acre,
Rio Branco - AC, Brazil
- 56 Herbario Alfredo Paredes, Universidad Central del Ecuador, Quito, Ecuador
- 57 Centro de Ciências Biológicas e da Natureza, Universidade Federal do Acre, Rio Branco - AC, Brazil
- 58 Laboratoire Évolution et Diversité Biologique - UMR 5174 (CNRS/IRD/UPS), CNRS, Toulouse,
France
- 59 Rougier-Gabon, Libreville, Gabon
- 60 Nicholas School of the Environment, Duke University, Durham, NC, USA
- 61 Grantham Research Institute on Climate Change and the Environment, London, UK
- 62 Inventory & Monitoring Program, National Park Service, Fredericksburg, VA, USA
- 63 Smithsonian Institution, Washington, DC, USA
- 64 Proyecto Castaña, Madre de Dios, Peru
- 65 Universidad Nacional de San Agustín de Arequipa, Arequipa, Peru
- 66 Instituto de Geociências, Faculdade de Meteorologia, Universidade Federal do Pará, Belém - PA,
Brazil
- 67 Faculty of Science, Department of Ecology and Environmental Sciences, Palacký University
Olomouc, Olomouc, Czech Republic
- 68 Center for Tropical Forest Science, Smithsonian Tropical Research Institute, Panama, Panama
- 69 Facultad de Ciencias Biológicas, Universidad Nacional de la Amazonía Peruana, Iquitos, Peru
- 70 Embrapa Genetic Resources & Biotechnology, Brazilian Agricultural Research Corporation
(EMBRAPA), Brasília, Brazil
- 71 Instituto de Investigaciones de la Amazonía Peruana, Iquitos, Peru
- 72 Ecologie des Forêts de Guyane (ECOFOG), CIRAD, Kourou, French Guiana

- 73 Department of Anthropology, The University of Texas at Austin, Austin, TX, USA
- 74 Forest Resources Management, Gembloux Agro-Bio Tech, University of Liège, Liège, Belgium
- 75 AMAP Lab, IRD, CIRAD, CNRS, INRA, Univ Montpellier, Montpellier, France
- 76 Socioecosistemas y Cambio Climatico, Fundacion con Vida, Medellín, Colombia
- 77 School of Forestry, Beijing Forestry University, Beijing, China
- 78 Institute of Biological Sciences, Universidade Federal do Pará, Belém - PA, Brazil
- 79 National Museum of Natural History, Smithsonian Institute, Washington, DC, USA
- 80 School of Geography, Earth and Environmental Sciences, University of Birmingham, Birmingham, UK
- 81 School of Geography, Earth and Environmental Sciences, University of Plymouth, Plymouth, UK
- 82 Embrapa Amazônia Oriental, Brazilian Agricultural Research Corporation (EMBRAPA), Brasília, Brazil
- 83 Universidad Nacional Jorge Basadre de Grohmann (UNJBG), Tacna, Peru
- 84 Forestry Research Institute of Ghana (FORIG), Kumasi, Ghana
- 85 Smithsonian Institution Forest Global Earth Observatory (ForestGEO), Smithsonian Tropical Research Institute, Washington, DC, USA
- 86 School of Biology, University of Leeds, Leeds, UK
- 87 128 Busbridge Lane, Godalming, Surrey, UK
- 88 Royal Botanic Garden Edinburgh, Edinburgh, UK
- 89 Lukuru Wildlife Research Foundation, Kinshasa, Democratic Republic of Congo
- 90 Division of Vertebrate Zoology, Yale Peabody Museum of Natural History, New Haven, CT, USA
- 91 Institute of Botany, Czech Academy of Sciences, Brno, Czech Republic
- 92 Department of Botany, Palacký University in Olomouc, Olomouc, Czech Republic
- 93 Instituto Venezolano de Investigaciones Científicas (IVIC), Caracas, Venezuela
- 94 Département Hommes, natures, sociétés, Muséum National d'Histoire Naturel, Paris, France
- 95 Universidad Nacional de San Antonio Abad del Cusco, Cusco, Peru
- 96 Biological and Environmental Sciences, University of Stirling, Stirling, UK
- 97 Instituto IMANI, Universidad Nacional de Colombia, Leticia, Colombia
- 98 Faculty of Science, Department of Botany and Plant Physiology, University of Buea, Buea, Cameroon
- 99 Department of Environment, Computational & Applied Vegetation Ecology (Cavelab), Ghent University, Ghent, Belgium
- 100 PELD, Universidade do Estado de Mato Grosso, Nova Xavantina-MT, Brazil
- 101 Tropical Peat Research Institute, Malaysian Palm Oil Board, Kuala Lumpur, Malaysia
- 102 Agteca, Santa Cruz, Bolivia
- 103 Graduate School of Agriculture, Kyoto University, Japan
- 104 Royal Botanic Gardens Kew, Richmond, London, UK
- 105 Department of Earth Sciences, University of Hong Kong, HKSAR
- 106 Centre for Tropical Environmental and Sustainability Science (TESS) and College of Marine and Environmental Sciences, James Cook University, Australia
- 107 Uganda Programme, Wildlife Conservation Society, Kampala, Uganda
- 108 Remote Sensing Division, National Institute for Space Research (INPE), São José dos Campos-SP, Brazil
- 109 Department of Ecology, University of Brasília, Brasília, Brazil
- 110 Environmental Science and Policy, George Mason University, Fairfax, VA, USA

- 111 Botany Department, University of Ibadan, Ibadan, Nigeria
- 112 Coordenação da Biodiversidade, Instituto Nacional de Pesquisas da Amazônia (INPA), Manaus, Brazil
- 113 cE3c – Centre for Ecology, Evolution and Environmental Changes / Azorean Biodiversity Group, Universidade dos Açores, Angra do Heroísmo, Azores, Portugal
- 114 LIBRe – Laboratory for Integrative Biodiversity Research, Finnish Museum of Natural History, University of Helsinki, Helsinki, Finland
- 115 Laboratório de Biogeoquímica Ambiental Wolfgang C. Pfeiffer, Universidade Federal de Rondônia, Porto Velho - RO, Brazil
- 116 Faculdade de Ciências Agrárias, Biológicas e Sociais Aplicadas, Universidad do Estado de Mato Grosso, Nova Xavantina-MT, Brazil
- 117 Tropical Forests and People Research Centre, University of the Sunshine Coast, Australia
- 118 Flamingo Land Ltd., North Yorkshire, UK
- 119 Centre for Ecology and Hydrology, Wallingford, UK
- 120 School of International Tropical Forestry, Universiti Malaysia Sabah, Kota Kinabalu, Malaysia
- 121 Escuela de Ciencias Forestales, Unidad Académica del Trópico, Universidad Mayor de San Simón, Sacta, Bolivia
- 122 Faculty of Science, Universiti Brunei Darussalam, Brunei
- 123 Agence Nationale des Parcs Nationaux, Libreville, Gabon
- 124 Ministère de la Forêt, de la Mer, de l'Environnement, Chargé du Plan Climat, Libreville, Gabon
- 125 University of Edinburgh, Edinburgh, UK
- 126 Biologia Vegetal, Universidade Estadual de Campinas, Campinas - SP, Brazil
- 127 Facultad de Ingeniería Ambiental, Universidad Estatal Amazónica, Puyo, Pastaza, Ecuador
- 128 Forest Research Centre, Sabah Forestry Department, Sepilok, Malaysia
- 129 Carrera de Ingeniería Forestal, Universidad Técnica del Norte, Ibarra, Ecuador
- 130 Royal Botanical Garden Edinburgh, Edinburgh, UK
- 131 Universidad Regional Amazónica IKIAM, Tena, Ecuador
- 132 Public Communications and Outreach Group, Parks and Recreation Division, Oakland Park, FL, USA
- 133 Keller Science Action Center, Field Museum, Chicago, IL, USA
- 134 Centre for Agricultural Research in Suriname (CELOS), Paramaribo, Suriname
- 135 Department of Forest Ecology and Forest Management Group, Wageningen University and Research, Wageningen, The Netherlands
- 136 University of Oslo, Oslo, Norway
- 137 Instituto de Ciencias Naturales, Universidad Nacional de Colombia, Leticia, Colombia
- 138 Department of Biology, Boston University, Boston, USA
- 139 Institute of Research for Forestry Development (INDEFOR), Universidad de los Andes, Mérida, Venezuela
- 140 Bureau Waardenburg, Culemborg, The Netherlands
- 141 Socioecosistemas y Cambio Climático, Fundación Con Vida, Medellín, Colombia
- 142 Centro de Conservación, Investigación y Manejo de Áreas Naturales, CIMA Cordillera Azul, Lima, Peru
- 143 Iwokrama International Centre for Rainforest Conservation and Development, Georgetown, Guyana
- 144 Carboforexpert, Geneva, Switzerland
- 145 Universidade Federal Rural da Amazônia/CAPES, Belém - PA, Brazil
- 146 Museu Paraense Emílio Goeldi, Belém - PA, Brazil
- 147 Faculty of Environmental Sciences and Natural Resource Management, Norwegian University of Life Sciences, Ås, Norway

- 148 Instituto Federal do Acre, Rio Branco - AC, Brazil
- 149 Universidad de San Antonio Abad del Cusco, Cusco, Peru
- 150 Guyana Forestry Commission, Georgetown, Guyana
- 151 Federal University of Alagoas, Maceió, Brazil
- 152 Sustainable Landscapes and Food Systems, Center for International Forestry Research, Bogor, Indonesia
- 153 Faculty of Forestry, University of British Columbia, Vancouver, Canada
- 154 Department of Forest Botany, Dendrology and Geobiocoenology, Mendel University in Brno, Brno, Czech Republic
- 155 Department of Plant & Soil Science, School of Biological Sciences, University of Aberdeen, Aberdeen, UK
- 156 Institute for Conservation Research, San Diego Zoo, San Diego, USA
- 157 UK Research & Innovation, Innovate UK, London
- 158 Department of Geography, National University of Singapore, Singapore, Singapore
- 159 Naturalis Biodiversity Center, Leiden, The Netherlands
- 160 Systems Ecology, VU University, Amsterdam, The Netherlands
- 161 Faculty of Forestry, University of Toronto, Toronto, Canada
- 162 Universidad de los Andes, Merida, Colombia
- 163 Wildlife Conservation Society, New York, NY, USA
- 164 Yale School of Forestry & Environmental Studies, Yale University, New Haven, CT, USA
- 165 School of Geography, University of Nottingham, Nottingham, UK
- 166 Van der Hout Forestry Consulting, Rotterdam, The Netherlands
- 167 Van Hall Larenstein University of Applied Sciences, Velp, The Netherlands
- 168 Utrecht University, Utrecht, The Netherlands
- 169 Deltares, Delft, The Netherlands
- 170 School of Environmental and Forest Sciences, University of Washington, Seattle, OR, USA
- 171 Department of Biological Sciences, Florida International University, Florida, FL, USA
- 172 Centro de Investigación y Promoción del Campesinado, La Paz, Bolivia
- 173 School of Earth Sciences and Environmental Sustainability, Northern Arizona University, Flagstaff, AZ, USA
- 174 Institut de Recherche en Ecologie Tropicale, Libreville, Gabon
- 175 School of Natural Sciences, University of Stirling, Stirling, UK
- 176 School of Natural Sciences, University of Bangor, Bangor, UK
- 177 University of Liberia, Monrovia, Liberia
- 178 Forest Management, Centre for Agricultural Research in Suriname (CELOS), Paramaribo, Suriname
- 179 Department of Geography and The Environment, University of Texas at Austin, Austin, TX, USA
- 180 Tropenbos International, Wageningen, The Netherlands
- 181 Biology, Utrecht University, Utrecht, The Netherlands

1 **Abstract**

2 The sensitivity of tropical forest carbon to climate is a key uncertainty in predicting global climate
3 change. While short-term drying and warming are known to impact forests it is unknown if such effects
4 translate into long-term responses. Here we analyse 590 permanent plots measured across the tropics to
5 derive the equilibrium climate controls on forest carbon. Maximum temperature is the most important
6 predictor of aboveground biomass ($-9.1 \text{ Mg C ha}^{-1} \text{ }^{\circ}\text{C}^{-1}$), primarily by reducing woody productivity, and
7 with a greater rate of decline in the hottest forests ($>32.2 \text{ }^{\circ}\text{C}$). Our results nevertheless reveal greater
8 thermal resilience than observations of short-term variation imply. To realise the long-term climate
9 adaptation potential of tropical forests requires both protecting them and stabilising the Earth's climate.

10

11 **One sentence summary.** Biome-wide variation in tropical forest carbon stocks and dynamics shows
12 long-term thermal resilience.

13 Main text

14 The response of tropical terrestrial carbon to environmental change is a critical component of global
15 climate models (1). Land-atmosphere feedbacks depend on the balance of positive biomass growth
16 stimulation by CO₂ fertilisation (i.e. β) and negative responses to warmer temperatures and any
17 change in precipitation (i.e. γ). Yet the climate response is so poorly constrained that it remains one of
18 the largest uncertainties in Earth system models (2, 3), with the temperature sensitivity of tropical land
19 carbon stocks alone differing by $> 100 \text{ Pg C } ^\circ\text{C}^{-1}$ among models (2). Such uncertainty impedes our
20 understanding of the global carbon cycle, limiting our ability to simulate the future of the Earth
21 system under different long-term climate mitigation strategies. A critical long-term control on tropical
22 land-atmosphere feedbacks is the sensitivity to climate (γ) of tropical forests, where c. 40 % of the
23 world's vegetation carbon resides (4).

24 The sensitivity to environmental change of tropical biomass carbon stocks, their rate of production
25 and their persistence, can all be estimated by relating their short-term and inter-annual responses to
26 variation in climate (5-7). These sensitivities are then used to constrain longer-term projections of
27 climate responses (2). Such approaches typically find that higher minimum temperatures are strongly
28 associated with slower tree growth and reduced forest carbon stocks, likely due to increased
29 respiration at higher temperatures (7-9). Tropical forest carbon is also sensitive to precipitation (10),
30 with, for example, elevated tree mortality occurring during drought events (11).

31 Yet the sensitivity of ecosystems to inter-annual fluctuations may be an unreliable guide to their
32 longer-term responses to climate change. Such responses will also be influenced by physiological
33 acclimation (12), changes in demographic rates (13), and shifts in species composition (14). For
34 example, both respiration and photosynthesis can acclimate under sustained temperature increases
35 (15-17), and tropical trees exhibit physiological plasticity (18) and shifts in species composition (14)
36 under sustained drought. These processes could mean that tropical forests are less sensitive to climate
37 than estimates derived from inter-annual variability imply. An alternative, complimentary approach to
38 assessing sensitivity to climate is to measure and analyse spatial variation in tropical ecosystems
39 across climate gradients as a space-for-time substitution. Such biome-wide spatial variation in forest

40 carbon stocks, fluxes and persistence offers a unique and largely unexplored window into the potential
41 equilibrium sensitivity of tropical forest vegetation to warming, as it captures real-world vegetation
42 responses that allow for physiological and ecological adaptation (12).

43 To assess the long-term climate controls on tropical forest growth and carbon stocks, here we have
44 assembled, measured, and analysed a pan-tropical network of 590 permanent, long-term inventory
45 plots (Fig. 1, see Figs. S1-2 for ability to capture biome climate space). Our analysis combines
46 standardised measurements from across South American, African, Asian and Australian tropical
47 lowland forests (273, 239, 61 and 17 plots respectively). For every plot we calculated aboveground
48 carbon stocks (19). Then, to better assess the dynamic controls on aboveground carbon stocks, we
49 also computed the rate of carbon gained by the system (aboveground woody carbon production,
50 calculated as tree growth plus newly recruited trees, in $\text{Mg C ha}^{-1} \text{ yr}^{-1}$), and the carbon residence time
51 in living biomass (calculated as the ratio of living C stocks to C gains, in years).

52 We find considerable variation in biomass carbon among continents, with lower stocks per unit area
53 in South America compared with the Paleotropics even after accounting for environmental variables
54 (Fig. 1). Continents with high carbon stocks had either large carbon gains (Asia), or long carbon
55 residence times (Africa, Fig. 1). Because of these differences among continents, which are potentially
56 due to differences in evolutionary history (20), we analyse the environmental drivers of spatial
57 variation in carbon stocks while accounting for biogeographical differences. We fitted linear models
58 with explanatory variables representing hypothesised mechanistic controls of climate on tropical
59 forest carbon (Table S1). We also included soil covariates, continent intercepts and eigenvectors
60 describing spatial relationships amongst plots to account for other sources of variation (21).

61 Forest carbon stocks were most strongly related to maximum temperature (-5.9% per 1°C increase in
62 maximum temperature, 95 % CI = -8.6 to -3.1% , Fig. 2, equivalent to $-9.1 \text{ Mg C ha}^{-1} \text{ }^\circ\text{C}^{-1}$ for a stand
63 with the mean carbon stocks in our dataset, $154.6 \text{ Mg C ha}^{-1}$), followed by rainfall ($+2.4\%$ per 100
64 mm increase in precipitation in the driest quarter, 95 % CI = 0.6 – 4.3% , Fig. 2, equivalent to 0.04
65 $\text{Mg C ha}^{-1} \text{ mm}^{-1}$ for a stand with the mean carbon stocks in our dataset), with no statistically
66 significant relationship with minimum temperature, wind speed or cloud cover (Fig 2). The effects of

67 maximum temperature and precipitation are also evident in an analysis considering a wider suite of
68 climate variables than those tied to hypothesised mechanisms (Fig. S3), and in an additional
69 independent pantropical dataset of 223 single-census plots (for which carbon gains and residence time
70 cannot be assessed, Fig. S4).

71 The negative effect of maximum temperature on aboveground carbon stocks mainly reflects reduced
72 carbon gains with increasing temperature (-4.0 % per 1°C, 95% CI = -6.2 to -1.8 %, Fig. 2) while the
73 positive effect of precipitation emerges through longer carbon residence times with increasing
74 precipitation in the driest quarter (3.3 % per 100 mm, 95 % CI = 0.9 – 5.7 %, Fig. 2). Carbon
75 residence time also increased with the proportion of clay in the soil (Fig. 2). The additive effects of
76 precipitation and temperature on carbon stocks were modified by an interaction between them (Δ AIC
77 = 15.4 comparing full linear model with or without interaction), with temperature effects more
78 negative when precipitation is low (Fig. S6). The interaction was through shortening carbon residence
79 time (Δ AIC = 11.9) rather than reducing carbon gains (model without interaction better, Δ AIC =
80 1.4).

81 An alternative analysis using decision tree algorithms (22) also showed maximum temperature and
82 precipitation to be important (Fig. S7). This decision tree approach, which can capture complex non-
83 linear relationships (22), indicated potential non-linearity in the relationships between carbon stocks
84 and both temperature and precipitation, with the positive effect of increasing dry season precipitation
85 on residence times strengthening when precipitation was low, and the negative effect of maximum
86 temperature intensifying at high temperatures (Fig. S7).

87 We further investigated non-linearity in the temperature relationship using breakpoint regression
88 (supported over linear regression based on lower AIC, Δ AIC = 15.0), which revealed that above 32.2
89 °C (95 % CI = 31.7 – 32.6 °C) the relationship between carbon stocks and maximum temperature
90 became more negative (cooler than breakpoint: -3.8 % °C⁻¹, warmer than breakpoint: -14.7 % °C⁻¹,
91 Fig. 3). By partitioning carbon stocks into their production and persistence we find that this non-
92 linearity reflects changes to carbon residence time (Δ AIC = 10.6) rather than gains (Δ AIC = 1.7).
93 Overall, our results thus indicate two separate climate controls on carbon stocks: a negative linear

94 effect of maximum temperature through reduced carbon gains, and a non-linear negative effect of
95 maximum temperature, ameliorated by high dry-season precipitation, through reduced carbon
96 residence time.

97 The effect of temperature on carbon residence time only emerges when dry season precipitation is low
98 so is consistent with theoretical expectations that negative effects of temperature on tree longevity are
99 exacerbated by moisture limitation, rather than being independent of it and due to increased
100 respiration costs alone (23). This could occur through high vapour pressure deficits in hot and dry
101 forests increasing mortality risk by causing hydraulic stress (23, 24), or carbon starvation due to
102 limited photosynthesis as a result of stomatal closure (23). Notably, the temperature-precipitation
103 interaction we find for aboveground stocks is in the opposite direction to temperature-precipitation
104 interactions reported for soil carbon. In soils, moisture limitation suppresses the temperature response
105 of heterotrophic respiration (25), while in trees moisture limitation enhances the mortality risks of
106 high temperatures.

107 The temperature effects on biomass carbon stocks and gains are primarily due to maximum rather
108 than minimum temperature. This is consistent with high daytime temperatures reducing CO₂
109 assimilation rates, for example due to increased photorespiration or longer duration of stomatal
110 closure (26, 27), whereas if negative temperature effects were to have increased respiration rates there
111 should be a stronger relationship with minimum (i.e. night-time) temperature. Critically, minimum
112 temperature is unrelated to aboveground carbon stocks both pan-tropically and in the one continent,
113 South America, where maximum and minimum temperature are largely decoupled ($r = 0.33$; Fig. S8).
114 While carbon gains are negatively related to minimum temperature (Fig S9) this bivariate relationship
115 is weaker than with maximum temperature, and disappears once the effects of other variables are
116 accounted for (Fig. 2). Finally, in Asia, the tropical region which experiences the warmest minimum
117 temperatures of all, both carbon stocks and carbon gains are highest (Fig. 1, Fig. S11).

118 Overall our results suggest that tropical forests have considerable potential to acclimate and adapt to
119 the effects of night-time minimum temperatures, but are clearly sensitive to the effects of daytime
120 maximum temperature. This is consistent with ecophysiological observations suggesting that the

121 acclimation potential of respiration (15) is greater than that of photosynthesis (17). The temperature
122 sensitivity revealed by our analysis is also considerably weaker than short-term sensitivities
123 associated with inter-annual climate variation (8). For example, by relating short-term annual climate
124 anomalies to responses in plots, the effect of a 1°C increase in temperature on carbon gains has been
125 estimated as more than three-fold our long-term, pantropical result (28). This stronger long-term
126 thermal resilience is likely due to a combination of individual acclimation and plasticity (15-17),
127 differences in species' climate responses (29) leading to shifts in community composition due to
128 changing demographic rates (12) and the immigration of species with higher performance at high
129 temperatures (12).

130 Our pantropical analysis of the sensitivity to climate of aboveground forest carbon stocks, gains and
131 persistence shows that warming reduces carbon stocks and gains from woody productivity. Using a
132 reference carbon stock map (30) and applying our estimated temperature sensitivity (including non-
133 linearity) while holding other variables constant leads to an eventual biome-wide reduction of 14.1 Pg
134 C in live biomass (including scaling to estimate carbon in roots) for a 1°C increase in maximum
135 temperature (95 % CI = 6.9 – 20.7 Pg). This compares with a large range of projected sensitivities in
136 the subset of coupled climate carbon cycle models that report vegetation carbon (1 – 58 Pg C °C⁻¹),
137 although we note that these models have not been run to equilibrium (see SI Methods).

138 Our results suggest that stabilising global surface temperatures at 2°C above pre-industrial levels will
139 cause a potential long-term biome-wide loss of 35.3 Pg C (95 % CI = 20.9 – 49.0 Pg, estimates with
140 alternative baseline biomass maps 24.0 – 28.4 Pg, Fig. S12). The greatest long-term reductions in
141 carbon stocks are projected in South America, where baseline temperatures and future warming are
142 both highest (Fig. 4, Fig. S13). This warming would push 71 % of the biome beyond the thermal
143 threshold – maximum temperature of 32.2°C – where larger long-term reductions in biomass are
144 expected (Fig. S14). Of course, growth stimulation by carbon dioxide (31) will partially or wholly
145 offset the effect of this temperature increase, depending on both the level of atmospheric carbon
146 dioxide that limits warming to 2°C above pre-industrial levels and the fertilization effect of this
147 carbon dioxide on tropical trees. Although CO₂ fertilisation is expected to reduce temperature induced

148 carbon losses from biomass across the tropics (Table S3), our analysis indicates that CO₂ fertilisation
149 is not enough to offset long-term temperature induced carbon losses within Amazonia (Fig. S15).

150 The long-term climate sensitivities derived from our pan-tropical field measurements incorporate
151 ecophysiological and ecological adaptation, and so provide an estimate of the long-term, quasi-
152 equilibrium, response of tropical vegetation to climate. We note that this thermal adaptation potential
153 may not be fully realised in future responses because (i) the speed of temperature rises may exceed
154 species' adaptive capabilities, (ii) habitat fragmentation may limit species' ability to track changes in
155 the environment, and (iii) other human impacts such as logging and fire can increase the vulnerability
156 of forest carbon stocks to high temperatures. While many tropical forests are under severe threat of
157 conversion, our results show that, in the long-run, tropical forests that remain intact can continue to
158 store high levels of carbon under high temperatures. Achieving the biome-wide climate resilience
159 potential we document depends on limiting heating and on large-scale conservation and restoration to
160 protect biodiversity and allow species to move.

161

162

163 **References and Notes**

- 164 1. P. M. Cox, R. A. Betts, C. D. Jones, S. A. Spall, I. J. Totterdell, Acceleration of global
165 warming due to carbon-cycle feedbacks in a coupled climate model. *Nature* **408**, 184 (2000).
- 166 2. P. M. Cox et al., Sensitivity of tropical carbon to climate change constrained by carbon
167 dioxide variability. *Nature* **494**, 341-344 (2013).
- 168 3. B. B. Booth et al., High sensitivity of future global warming to land carbon cycle
169 processes. *Environmental Research Letters* **7**, 024002 (2012).
- 170 4. K.-H. Erb et al., Unexpectedly large impact of forest management and grazing on global
171 vegetation biomass. *Nature* **553**, 73 (2017).
- 172 5. W. Wang et al., Variations in atmospheric CO₂ growth rates coupled
173 with tropical temperature. *Proceedings of the National Academy of Sciences* **110**, 13061
174 (2013).
- 175 6. J. Liu et al., Contrasting carbon cycle responses of the tropical continents to the 2015–2016
176 El Niño. *Science* **358**, eaam5690 (2017).
- 177 7. D. A. Clark, S. C. Piper, C. D. Keeling, D. B. Clark, Tropical rain forest tree growth and
178 atmospheric carbon dynamics linked to interannual temperature variation during 1984–2000.
179 *Proceedings of the National Academy of Sciences* **100**, 5852 (2003).
- 180 8. W. R. L. Anderegg et al., Tropical nighttime warming as a dominant driver of variability in
181 the terrestrial carbon sink. *Proceedings of the National Academy of Sciences* **112**, 15591-
182 15596 (2015).
- 183 9. A. Ballantyne et al., Accelerating net terrestrial carbon uptake during the warming hiatus due
184 to reduced respiration. *Nature Climate Change* **7**, 148 (2017).
- 185 10. J. K. Green et al., Large influence of soil moisture on long-term terrestrial carbon uptake.
186 *Nature* **565**, 476-479 (2019).
- 187 11. O. L. Phillips et al., Drought Sensitivity of the Amazon Rainforest. *Science* **323**, 1344 (2009).
- 188 12. M. D. Smith, A. K. Knapp, S. L. Collins, A framework for assessing ecosystem dynamics in
189 response to chronic resource alterations induced by global change. *Ecology* **90**, 3279-3289
190 (2009).
- 191 13. J. H. Brown, T. J. Valone, C. G. Curtin, Reorganization of an arid ecosystem in response to
192 recent climate change. *Proceedings of the National Academy of Sciences* **94**, 9729-9733
193 (1997).
- 194 14. S. Fauset et al., Drought-induced shifts in the floristic and functional composition of tropical
195 forests in Ghana. *Ecol Lett* **15**, 1120-1129 (2012).
- 196 15. A. Gunderson Carla, H. O'Hara Keiran, M. Champion Christina, V. Walker Ashley, T.
197 Edwards Nelson, Thermal plasticity of photosynthesis: the role of acclimation in forest
198 responses to a warming climate. *Global Change Biology* **16**, 2272-2286 (2010).
- 199 16. M. Slot et al., Thermal acclimation of leaf respiration of tropical trees and lianas: response to
200 experimental canopy warming, and consequences for tropical forest carbon balance. *Global*
201 *Change Biology* **20**, 2915-2926 (2014).
- 202 17. F. Ow Lai, L. Griffin Kevin, D. Whitehead, S. Walcroft Adrian, H. Turnbull Matthew,
203 Thermal acclimation of leaf respiration but not photosynthesis in *Populus deltoides* × *nigra*.
204 *New Phytologist* **178**, 123-134 (2008).
- 205 18. T. F. Domingues et al., Ecophysiological plasticity of Amazonian trees to long-term drought.
206 *Oecologia* **187**, 933-940 (2018).
- 207 19. See supplementary material.
- 208 20. J. W. F. Slik et al., Phylogenetic classification of the world's tropical forests. *Proceedings of*
209 *the National Academy of Sciences* **115**, 1837 (2018).
- 210 21. S. Dray, P. Legendre, P. R. Peres-Neto, Spatial modelling: a comprehensive framework for
211 principal coordinate analysis of neighbour matrices (PCNM). *Ecological Modelling* **196**, 483-
212 493 (2006).
- 213 22. L. Breiman, Random Forests. *Machine Learning* **45**, 5-32 (2001).
- 214 23. N. McDowell et al., Drivers and mechanisms of tree mortality in moist tropical forests. *New*
215 *Phytologist* **219**, 851-869 (2018).

- 216 24. G. Fontes Clarissa et al., Dry and hot: the hydraulic consequences of a climate change–type
 217 drought for Amazonian trees. *Philosophical Transactions of the Royal Society B: Biological*
 218 *Sciences* **373**, 20180209 (2018).
- 219 25. P. Ciais et al., Europe-wide reduction in primary productivity caused by the heat and drought
 220 in 2003. *Nature* **437**, 529-533 (2005).
- 221 26. M. E. Dusenge, A. G. Duarte, D. A. Way, Plant carbon metabolism and climate change:
 222 elevated CO₂ and temperature impacts on photosynthesis, photorespiration and respiration.
 223 *New Phytologist* **221**, 32-49 (2019).
- 224 27. S. Pau, M. Detto, Y. Kim, C. J. Still, Tropical forest temperature thresholds for gross primary
 225 productivity. *Ecosphere* **9**, e02311 (2018).
- 226 28. D. A. Clark, D. B. Clark, S. F. Oberbauer, Field-quantified responses of tropical rainforest
 227 aboveground productivity to increasing CO₂ and climatic stress, 1997-2009. *J. Geophys.*
 228 *Res.-Biogeosci.* **118**, 783-794 (2013).
- 229 29. W. R. L. Anderegg et al., Hydraulic diversity of forests regulates ecosystem resilience during
 230 drought. *Nature* **561**, 538-541 (2018).
- 231 30. V. Avitabile et al., An integrated pan-tropical biomass map using multiple reference datasets.
 232 *Global Change Biology* **22**, 1406-1420 (2016).
- 233 31. S. Piao et al., Evaluation of terrestrial carbon cycle models for their response to climate
 234 variability and to CO₂ trends. *Global Change Biology* **19**, 2117-2132 (2013).
- 235
- 236 References in SI only:
- 237 32. A. B. Anderson, White-sand vegetation of Brazilian Amazonia. *Biotropica* **13**, 199-210
 238 (1981).
- 239 33. S. R. Pezeshki, Root responses of flood-tolerant and flood-sensitive tree species to soil redox
 240 conditions. *Trees* **5**, 180-186 (1991).
- 241 34. O. L. Phillips, T. R. Baker, T. R. Feldpausch, R. J. W. Brienen, "RAINFOR Field Manual for
 242 Plot Establishment and Remeasurement," (2001).
- 243 35. J. Talbot et al., Methods to estimate aboveground wood productivity from long-term forest
 244 inventory plots. *Forest Ecology and Management* **320**, 30-38 (2014).
- 245 36. D. B. Clark, D. A. Clark, Landscape-scale variation in forest structure and biomass in a
 246 tropical rain forest. *Forest ecology and management* **137**, 185-198 (2000).
- 247 37. G. Lopez-Gonzalez, S. L. Lewis, M. Burkitt, O. L. Phillips, ForestPlots.net: a web application
 248 and research tool to manage and analyse tropical forest plot data. *Journal of Vegetation*
 249 *Science* **22**, 610-613 (2011).
- 250 38. G. Lopez-Gonzalez, S. L. Lewis, M. Burkitt, T. R. Baker, O. L. Phillips.
 251 (www.forestplots.net, 2009).
- 252 39. R. J. W. Brienen et al., Long-term decline of the Amazon carbon sink. *Nature* **519**, 344-348
 253 (2015).
- 254 40. J. Chave et al., Improved allometric models to estimate the aboveground biomass of tropical
 255 trees. *Global Change Biology* **20**, 3177-3190 (2014).
- 256 41. J. Chave et al., Towards a worldwide wood economics spectrum. *Ecology Letters* **12**, 351-366
 257 (2009).
- 258 42. A. E. Zanne et al. (Dryad Data Repository, 2009).
- 259 43. R. C. Goodman et al., Amazon palm biomass and allometry. *Forest Ecology and*
 260 *Management* **310**, 994-1004 (2013).
- 261 44. M. J. P. Sullivan et al., Field methods for sampling tree height for tropical forest biomass
 262 estimation. *Methods in Ecology and Evolution* **9**, 1179-1189 (2018).
- 263 45. S. C. Thomas, Asymptotic height as a predictor of growth and allometric characteristics in
 264 malaysian rain forest trees. *American Journal of Botany* **83**, 556-566 (1996).
- 265 46. T. R. Feldpausch et al., Tree height integrated into pantropical forest biomass estimates.
 266 *Biogeosciences* **9**, 3381-3403 (2012).
- 267 47. T. S. Kohyama, T. I. Kohyama, D. Sheil, Definition and estimation of vital rates from
 268 repeated censuses: Choices, comparisons and bias corrections focusing on trees. *Methods in*
 269 *Ecology and Evolution* **9**, 809-821 (2018).

- 270 48. A. R. Martin, M. Doraisami, S. C. Thomas, Global patterns in wood carbon concentration
271 across the world's trees and forests. *Nature Geoscience* **11**, 915-920 (2018).
- 272 49. D. Galbraith et al., Residence times of woody biomass in tropical forests. *Plant Ecology &*
273 *Diversity* **6**, 139-157 (2013).
- 274 50. G. Lopez-Gonzalez, M. J. P. Sullivan, T. R. Baker. (2015).
- 275 51. S. E. Fick, R. J. Hijmans, WorldClim 2: new 1-km spatial resolution climate surfaces for
276 global land areas. *International Journal of Climatology* **37**, 4302-4315 (2017).
- 277 52. R. J. Hijmans, S. Phillips, J. Leathwick, J. Elith, dismo: Species distribution modeling. R
278 package version 1.0-12. The R Foundation for Statistical Computing, Vienna [http://cran.r-](http://cran.r-project.org)
279 [project.org](http://cran.r-project.org), (2015).
- 280 53. A. M. Wilson, W. Jetz, Remotely Sensed High-Resolution Global Cloud Dynamics for
281 Predicting Ecosystem and Biodiversity Distributions. *PLOS Biology* **14**, e1002415 (2016).
- 282 54. M. New, D. Lister, M. Hulme, I. Makin, A high-resolution data set of surface climate over
283 global land areas. *Climate research* **21**, 1-25 (2002).
- 284 55. T. Hengl et al., SoilGrids250m: Global gridded soil information based on machine learning.
285 *PLOS ONE* **12**, e0169748 (2017).
- 286 56. P. R. Peres-Neto, P. Legendre, Estimating and controlling for spatial structure in the study of
287 ecological communities. *Global Ecology and Biogeography* **19**, 174-184 (2010).
- 288 57. S. L. Lewis et al., Increasing carbon storage in intact African tropical forests. *Nature* **457**,
289 1003 (2009).
- 290 58. K. Barton, 2015.
- 291 59. V. M. R. Muggeo, Estimating regression models with unknown break-points. *Statistics in*
292 *Medicine* **22**, 3055-3071 (2003).
- 293 60. A. Liaw, M. Wiener, Classification and Regression by randomForest. *R News* **2**, 18-22
294 (2002).
- 295 61. D. M. Olson et al., Terrestrial Ecoregions of the World: A New Map of Life on Earth A new
296 global map of terrestrial ecoregions provides an innovative tool for conserving biodiversity.
297 *BioScience* **51**, 933-938 (2001).
- 298 62. M. C. Hansen et al., High-Resolution Global Maps of 21st-Century Forest Cover Change.
299 *Science* **342**, 850-853 (2013).
- 300 63. R. Jackson et al., A global analysis of root distributions for terrestrial biomes. *Oecologia* **108**,
301 389-411 (1996).
- 302 64. S. S. Saatchi et al., Benchmark map of forest carbon stocks in tropical regions across three
303 continents. *Proceedings of the National Academy of Sciences* **108**, 9899-9904 (2011).
- 304 65. A. Baccini et al., Estimated carbon dioxide emissions from tropical deforestation improved by
305 carbon-density maps. *Nature Climate Change* **2**, 182-185 (2012).
- 306 66. E. T. A. Mitchard et al., Uncertainty in the spatial distribution of tropical forest biomass: a
307 comparison of pan-tropical maps. *Carbon Balance and Management* **8**, 10 (2013).
- 308 67. E. T. Mitchard et al., Markedly divergent estimates of Amazon forest carbon density from
309 ground plots and satellites. *Global Ecology and Biogeography* **23**, 935-946 (2014).
- 310 68. R. J. Hijmans. (2005). WorldClim - Global Climate Data. www.worldclim.org.
- 311 69. R. J. Hijmans, S. E. Cameron, J. L. Parra, P. G. Jones, A. Jarvis, Very high resolution
312 interpolated climate surfaces for global land areas. *International Journal of Climatology* **25**,
313 1965-1978 (2005).
- 314 70. B. Kirtman et al., Near-term climate change: projections and predictability. (2013).
- 315 71. H. D. Matthews, K. Caldeira, Stabilizing climate requires near-zero emissions. *Geophysical*
316 *Research Letters* **35**, (2008).
- 317 72. M. Meinshausen et al., The RCP greenhouse gas concentrations and their extensions from
318 1765 to 2300. *Climatic Change* **109**, 213 (2011).
- 319 73. W. Kolby Smith et al., Large divergence of satellite and Earth system model estimates of
320 global terrestrial CO₂ fertilization. *Nature Climate Change* **6**, 306 (2015).
- 321 74. D. W. Kicklighter et al., A first-order analysis of the potential role of CO₂ fertilization to
322 affect the global carbon budget: a comparison of four terrestrial biosphere models. *Tellus B:*
323 *Chemical and Physical Meteorology* **51**, 343-366 (1999).

- 324 75. Y. Malhi et al., The linkages between photosynthesis, productivity, growth and biomass in
325 lowland Amazonian forests. *Global Change Biology* **21**, 2283-2295 (2015).
- 326 76. C. Terrer et al., Nitrogen and phosphorus constrain the CO₂ fertilization of global plant
327 biomass. *Nature Climate Change* **9**, 684-689 (2019).
- 328 77. S. Wenzel, P. M. Cox, V. Eyring, P. Friedlingstein, Emergent constraints on climate-carbon
329 cycle feedbacks in the CMIP5 Earth system models. *Journal of Geophysical Research:*
330 *Biogeosciences* **119**, 794-807 (2014).
- 331 78. K. E. Taylor, R. J. Stouffer, G. A. Meehl, An overview of CMIP5 and the experiment design.
332 *Bulletin of the American Meteorological Society* **93**, 485-498 (2012).
- 333 79. The CMIP5 model data is available via the Earth System Grid Federation.
- 334 80. E. Bartholome, A. S. Belward, GLC2000: a new approach to global land cover mapping from
335 Earth observation data. *International Journal of Remote Sensing* **26**, 1959-1977 (2005).
- 336 81. J. Chave et al., Tree allometry and improved estimation of carbon stocks and balance in
337 tropical forests. *Oecologia* **145**, 87-99 (2005).
- 338 82. M. Slot, K. Winter, In situ temperature response of photosynthesis of 42 tree and liana species
339 in the canopy of two Panamanian lowland tropical forests with contrasting rainfall regimes.
340 *New Phytologist* **214**, 1103-1117 (2017).
- 341 83. Y. Malhi, The productivity, metabolism and carbon cycle of tropical forest vegetation.
342 *Journal of Ecology* **100**, 65-75 (2012).
- 343 84. E. A. Graham, S. S. Mulkey, K. Kitajima, N. G. Phillips, S. J. Wright, Cloud cover limits net
344 CO₂ uptake and growth of a rainforest tree during tropical rainy seasons. *Proceedings of the*
345 *National Academy of Sciences* **100**, 572-576 (2003).
- 346 85. W. F. Laurance, T. J. Curran, Impacts of wind disturbance on fragmented tropical forests: A
347 review and synthesis. *Austral Ecology* **33**, 399-408 (2008).

348

349

350 **Acknowledgements:** This paper is a product of the RAINFOR, AfriTRON and T-FORCES networks,
 351 and is facilitated by ForestPlots.net technology for data management which promotes science
 352 synergies across countries and continents. While these initiatives have been supported by numerous
 353 people and grants since their inception we are particularly indebted to hundreds of institutions, field
 354 assistants and local communities for help in establishing and maintaining the plots. For additional
 355 assistance with access to datasets we thank Jon Lloyd, Carlos Quesada, Michel Baisie, Olaf Banki,
 356 Wemo Betian, Vincent Bezar, Rene Boot, Mireille Breuer-Ndoundou Hockemba, Ezequiel Chavez,
 357 Douglas Daly, Armandu Daniels, Darcy Galiano Cabrera, Toby Gardner, Paolo Graca, Andrew
 358 Graham, Olivier Hardy, Eduardo Hase, David Hilvert, Muhammad Idhamsyah, Phillipe Jeanmart,
 359 Cisquet Keibou Opepa, Jeanette Kemp, Wilmar Lopez Oviedo, Jean-Remy Makana, Faustin Mbaya
 360 Mpanya Lukasu, Irina Mendoza Polo, Edi Mirmanto, Sam Moore, Jacques Mukinzi, Pétrus Naisso,
 361 Lucas Ojo, Raimunda Oliveira de Araújo, Sonia Cesarina Palacios Ramos, Alexander Parada
 362 Gutierrez, Guido Pardo, Marielos Peña-Claros, Freddy Ramirez Arevalo, Antonio Lima, Rodrigo
 363 Sierra, Natalino Silva, Marc Steininger, Marisol Toledo, John Tshibamba Mukendi, Darlington
 364 Tuagben, Hannsjoerg Woell and Ishak Yassir. We thank Jon Lloyd, Carlos Quesada for discussions
 365 and three anonymous reviewers for helpful comments and suggestions. **Funding:** The networks have
 366 been supported by multiple grants, most notably the European Research Council (ERC Advanced
 367 Grant 291585 – ‘T-FORCES’), the Gordon and Betty Moore Foundation (#1656 ‘RAINFOR’ and
 368 Monitoring Protected Areas in Peru to Increase Forest Resilience to Climate Change), the David and
 369 Lucile Packard Foundation, the European Union’s Seventh Framework Programme (283080 –
 370 ‘GEOCARBON’, 282664 – ‘AMAZALERT’), the Natural Environment Research Council (NERC
 371 grants NE/D005590/1 – ‘TROBIT’, NE/F005806/1 – ‘AMAZONICA’, ‘PPFOR’ E/M0022021/1,
 372 NERC Urgency Grants to O.L.P., and NERC New Investigators Grant to S.L.L. and T.F.), the NERC/
 373 State of São Paulo Research Foundation (FAPESP) consortium grants ‘BIO-RED’ (NE/N012542/1,
 374 2012/51872-5) and ‘ECOFOR’ (NE/K016431/1, 2012/51509-8), the Royal Society, the Centre for
 375 International Forestry (CIFOR) and Gabon’s National Parks Agency (ANPN). Additional data were
 376 included from the Tropical Ecology Assessment and Monitoring (TEAM) Network, a collaboration
 377 between Conservation International, the Missouri Botanical Garden, the Smithsonian Institution and
 378 the Wildlife Conservation Society, and partly funded by these institutions, the Gordon and Betty
 379 Moore Foundation, and other donors. M.J.P.S. was supported by the ERC (T-FORCES), NERC
 380 (‘BIO-RED’) and the Royal Society (CH160091), S.L.L. by a Royal Society University Research
 381 Fellowship, ERC Advanced Grant and a Phillip Leverhulme Prize, and O.L.P. by an ERC Advanced
 382 Grant, a Royal Society Wolfson Research Merit Award, and a Royal Society Global Challenges
 383 Award (‘FORAMA’, ICA/R1/180100). We thank the National Council for Science and Technology
 384 Development of Brazil (CNPq) for support to the Cerrado/Amazonia Transition Long-Term Ecology
 385 Project (PELD/403725/2012-7), the PPBio Phytogeography of Amazonia/Cerrado Transition project
 386 (CNPq/PPBio/457602/2012-0) and a Productivity Grant to B.S.M. and B.H.M-J.. Funding for plots in
 387 the Udzungwa Mountains (Tanzania) was obtained from the Leverhulme Trust under the Valuing the
 388 Arc project. This study is contribution number XXX to the Technical Series (TS) of the BDFFP
 389 (INPA – STRI). Data from RAINFOR, AfriTRON and T-FORCES are stored and curated by
 390 ForestPlots.net, a cyber-infrastructure initiative developed at the University of Leeds that unites
 391 permanent plot records and their contributing scientists from the world’s tropical forests. The
 392 development of ForestPlots.net and curation of most data analysed here was funded by several grants
 393 to O.L.P. (principally from NERC NE/B503384/1, NE/N012542/1 BIO-RED, ERC AdG 291585 T-
 394 FORCES’, and Gordon and Betty Moore Foundation #1656, ‘RAINFOR’), E.G. (‘GEOCARBON’,
 395 and NE/F005806/1 ‘AMAZONICA’), T.R.B. (Gordon and Betty Moore Foundation ‘Monitoring
 396 Protected Areas in Peru to Increase Forest Resilience to Climate Change’), S.L.L. (Royal Society
 397 University Research Fellowship; NERC New Investigators Award; Phillip Leverhulme Prize), and
 398 D.G. (NERC NE/N004655/1, ‘TREMOR’). **Author contributions:** O.L.P., S.L.L. and Y.M.
 399 conceived the RAINFOR, AfriTRON and T-FORCES forest census network programmes; M.J.P.S.,
 400 O.L.P. and S.L.L. conceived and designed the study. L.A., A.A.-M., T.R.B., R.J.W.B., S.K.B., K.A-

401 B., F.C., C.C., E.A.D., A.C.S., C.E.N.E., T.R.F., W.H., S.L.L., A.M.M., B.S.M., O.L.P., L.Q., B.S.,
402 T.S., R.V. and L.J.T.W. coordinated data collection with the help of most co-authors. O.L.P., T.R.B.,
403 G.L.-G. and S.L.L. conceived and managed ForestPlots.net; O.L.P., T.R.B., D.G., E.G. and S.L.L.
404 funded it, and R.B., T.F., G.L.-G., A.L., G.C.P. and M.J.P.S. helped develop it. M.J.P.S., T.R.B.,
405 W.H., S.L.L., A.E.-M., and L.Q. contributed tools to analyse data. All authors collected or supported
406 the collection of field data, M.J.P.S. analysed the data, M.J.P.S., O.L.P. and S.L.L. wrote the
407 manuscript with contributions from other authors. All co-authors commented on or approved the
408 manuscript. **Competing interests:** The authors declare no competing financial interests. **Data and**
409 **materials availability:** Plot-level input data and R scripts will be deposited as a data package on
410 ForestPlots.net (doi-xxx).

411

412 **Supplementary Materials:**

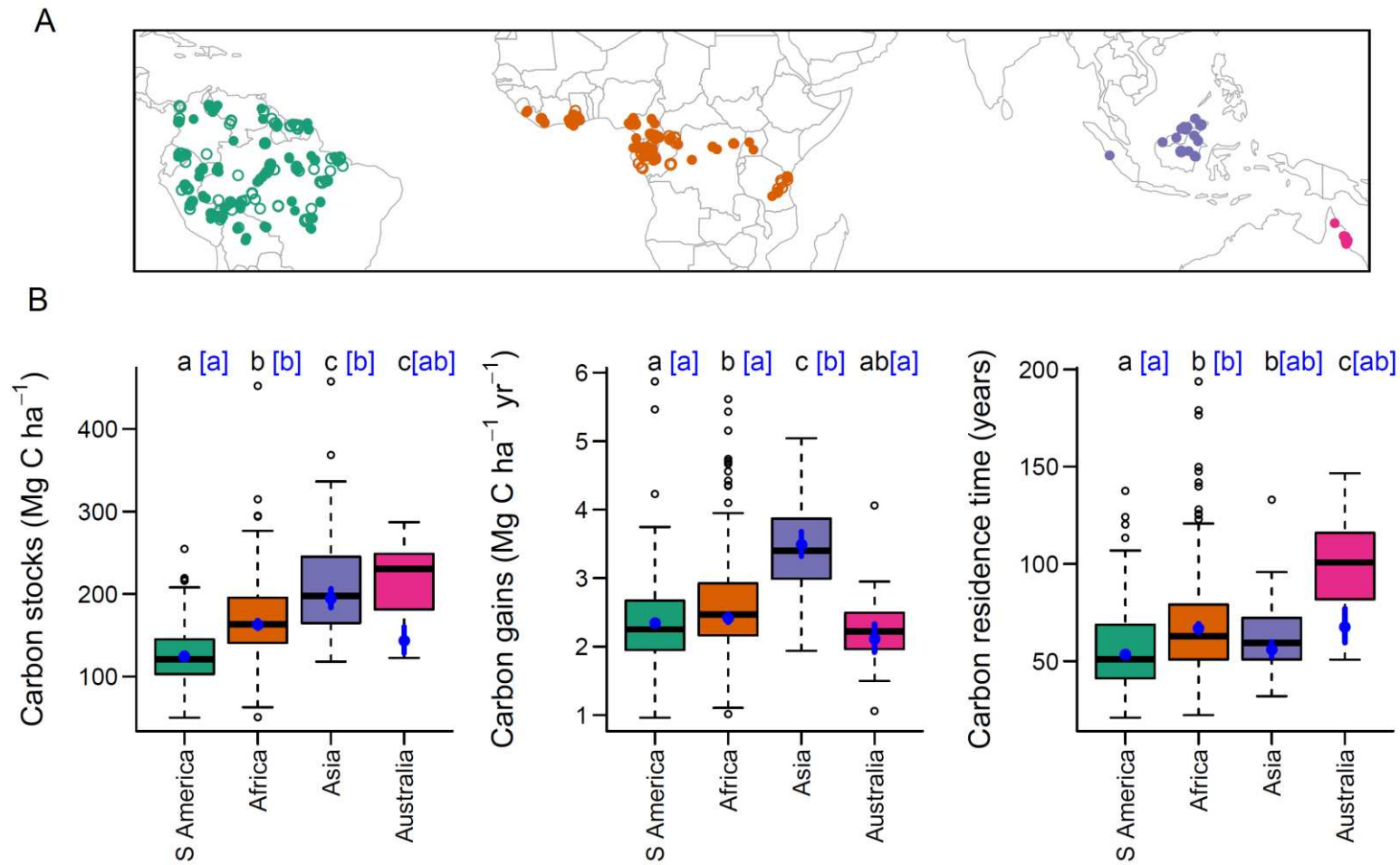
413 Materials and Methods

414 Figures S1-S15

415 Tables S1-S3

416 References (32-85)

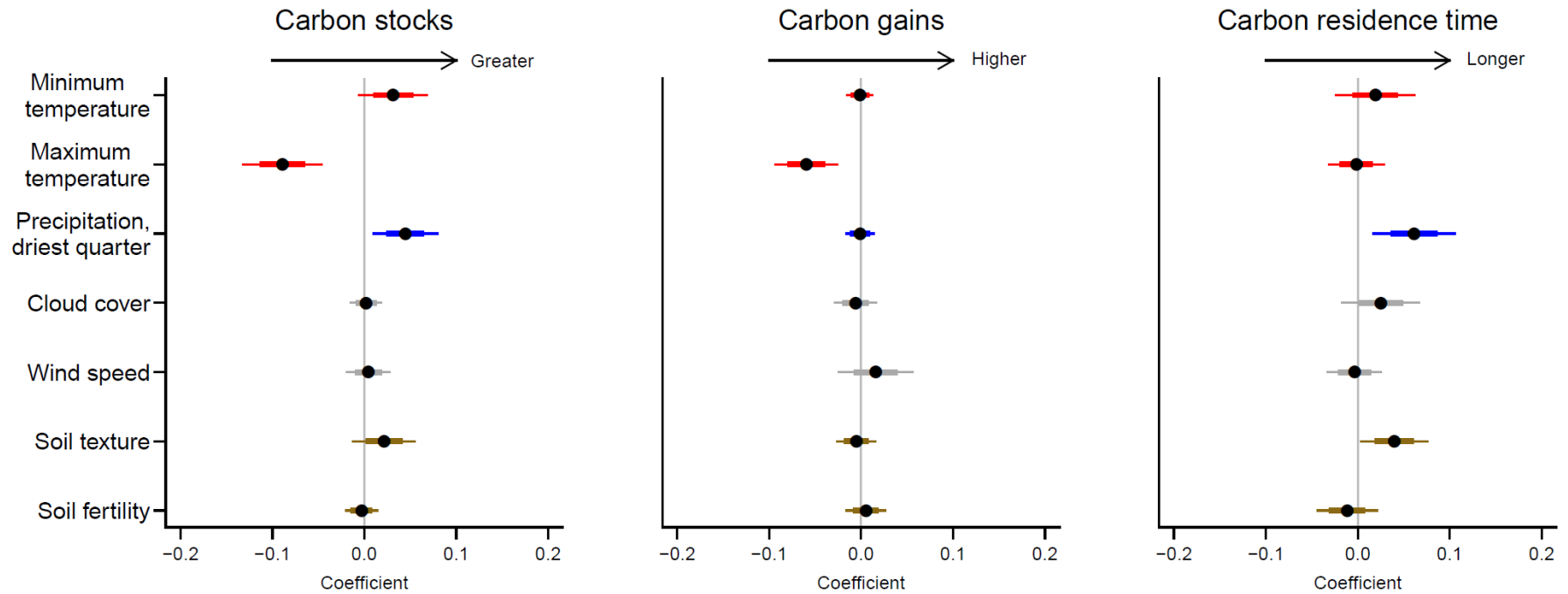
417



418

419 **Figure 1.** Spatial variation in tropical forest carbon. (A) Our plot network. Filled symbols show multi-census plots used in the main analysis, open symbols
 420 show single-census plots used as an independent dataset. (B) Variation in carbon among continents. Boxplots show raw variation while blue points show
 421 estimated mean values (\pm SE) after accounting for environmental variation. Letters denote statistically significant differences between continents ($P < 0.05$)
 422 based on raw data (black) or accounting for environmental effects (blue, square brackets).

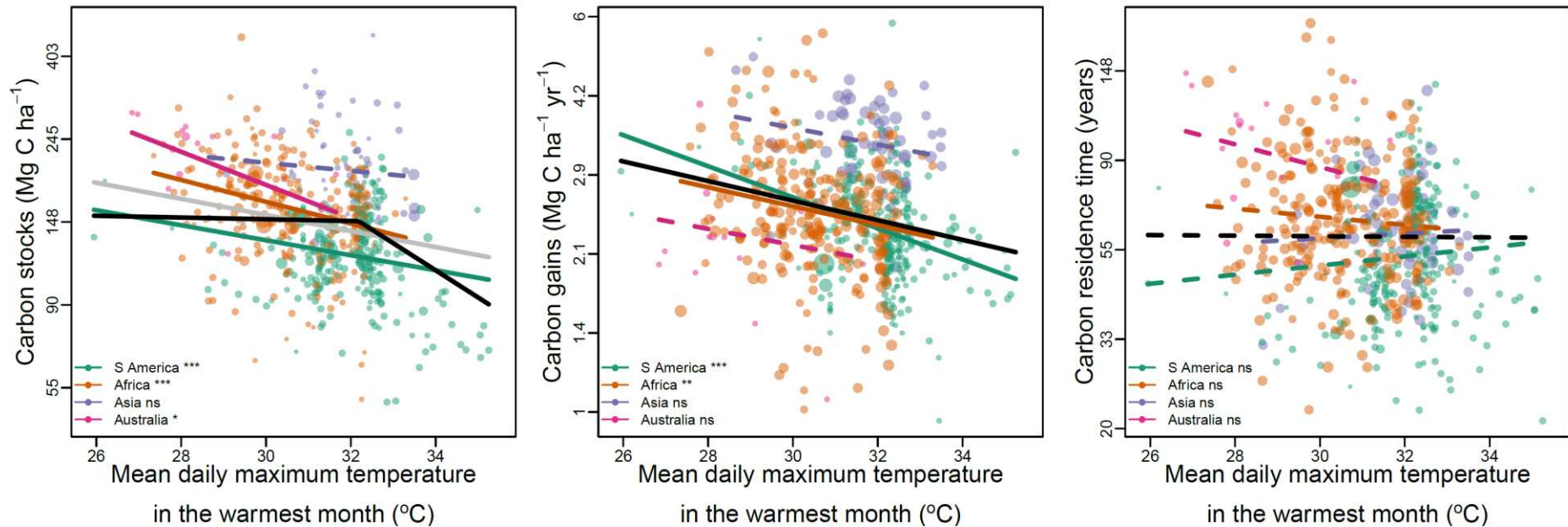
423
424
425
426



427

428 **Figure 2.** Correlates of spatial variation in tropical forest carbon. Points show coefficients from model-averaged general linear models. Variables that did not
429 occur in well-supported models are shrinkage adjusted towards zero. Coefficients are standardised so that they represent change in the response variable for
430 one standard deviation change in the explanatory variable. Error bars show standard errors (thick lines) and 95% confidence intervals (thin lines). Soil texture
431 is represented by the percentage clay, and soil fertility by cation exchange capacity. The full models explained 44.1 %, 31.4 % and 30.9 % of spatial variation
432 in carbon stocks, gains and residence time respectively. Coefficients are shown in Table S2. Results are robust to using an alternative allometry to estimate
433 tree biomass (Fig. S5).

434

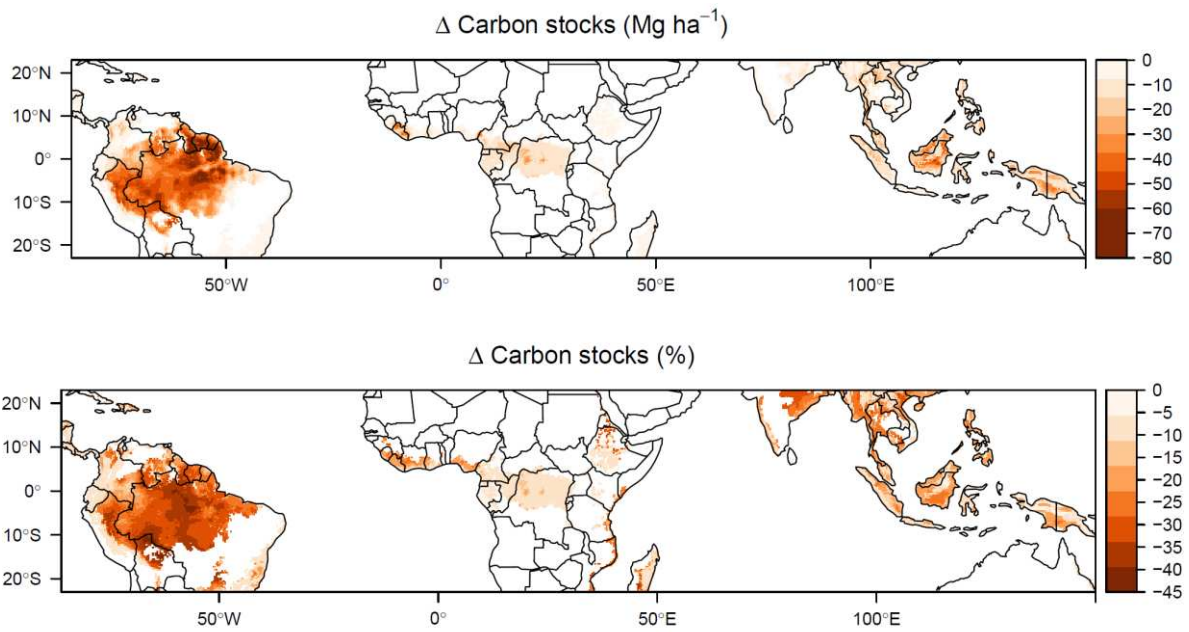


435

436

437 **Figure 3.** Temperature effects on tropical forest carbon stocks, carbon gains from woody productivity and carbon residence time. Black lines show the best
 438 pan-tropical relationships accounting for environmental covariates. The grey line shows the additional linear pan-tropical relationship for carbon stocks.
 439 Coloured lines show bivariate relationships within each continent. Statistically significant relationships are shown with solid lines, non-significant with
 440 dashed lines. Note that the y-axis is on a log-scale. Symbol point size is proportional to weights used in model fitting based on plot size and monitoring
 441 length, see SI Materials and Methods. For stocks and gains linear and break-point pan-tropical relationships are all statistically significant ($P < 0.001$), as are
 442 better sampled continents. For carbon residence time, relationships with temperature are non-significant but there is a statistically significant interaction
 443 between maximum temperature and precipitation in the driest quarter (Figure S6). Relationships with other variables are shown in Fig. S8-S10. *** $P <$
 444 0.001 , ** $P < 0.01$, * $P < 0.05$, ns $P \geq 0.05$

445



446

447 **Figure 4.** Long-term change in carbon stocks due to global surface temperature warming of
448 approximately 2°C. Maps show the predicted absolute and relative change in tropical forest carbon
449 stocks. Note that parts of the biome become warmer than currently observed in our dataset (Fig. S14).
450 See Fig. S12 for predictions using alternative carbon reference maps. Predictions are based on
451 temperature alone and do not include precipitation changes (for which future patterns of change are
452 uncertain) or potential moderation via elevated CO₂ (see Fig. S15 for analysis incorporating this).

453

454

455 **Supporting information for Long-term thermal Sensitivity of the Earth's Tropical**456 **Forests**

457 Martin J. P. Sullivan^{1,2}, Simon L. Lewis^{1,3}, Kofi Affum-Baffoe⁴, Carolina Castilho⁵, Flávia Costa⁶, Aida
458 Cuni Sanchez^{7,8}, Corneille E. N. Ewango^{9,10,11}, Wannes Hubau^{1,12,13}, Beatriz Marimon¹⁴, Abel Monteagudo-
459 Mendoza¹⁵, Lan Qie¹⁶, Bonaventure Sonké¹⁷, Rodolfo Vasquez Martinez¹⁵, Timothy R Baker¹, Roel J. W.
460 Brienen¹, Ted R. Feldpausch¹⁸, David Galbraith¹, Manuel Gloor¹, Yadvinder Malhi¹⁹, Shin-Ichiro Aiba²⁰,
461 Miguel N. Alexiades²¹, Everton C. Almeida²², Edmar Almeida de Oliveira²³, Esteban Álvarez Dávila²⁴,
462 Patricia Alvarez Loayza²⁵, Ana Andrade²⁶, Simone Aparecida Vieira²⁷, Luiz Aragão²⁸, Alejandro Araujo-
463 Murakami²⁹, Eric J.M.M. Arets³⁰, Luzmila Arroyo³¹, Peter Ashton³², Gerardo Aymard C.³³, Fabrício B.
464 Baccaro³⁴, Lindsay F. Banin³⁵, Christopher Baraloto³⁶, Plínio Barbosa Camargo³⁷, Jos Barlow³⁸, Jorcely
465 Barroso³⁹, Jean-François Bastin⁴⁰, Sarah A. Batterman^{1,41,42,43}, Hans Beeckman¹², Serge K. Begne^{17,44}, Amy
466 C. Bennett⁴⁴, Erika Berenguer^{19,38}, Nicholas Berry⁴⁵, Lilian Blanc⁴⁶, Pascal Boeckx⁴⁷, Jan Bogaert⁴⁸, Damien
467 Bonal⁴⁹, Frans Bongers⁵⁰, Matt Bradford⁵¹, Francis Q. Brearley², Terry Brncic⁵², Foster Brown⁵³, Benoit
468 Burban⁵⁴, José Luís Camargo²⁶, Wendeson Castro⁵⁵, Carlos Céron⁵⁶, Sabina Cerruto Ribeiro⁵⁷, Victor
469 Chama Moscoso¹⁵, Jérôme Chave⁵⁸, Eric Chezeaux⁵⁹, Connie J. Clark²⁵, Fernanda Coelho¹, Murray
470 Collins⁶¹, James A. Comiskey^{62,63}, Fernando Cornejo Valverde⁶⁴, Massiel Corrales Medina⁶⁵, Lola da
471 Costa⁶⁶, Martin Dančák⁶⁷, Greta C. Dargie¹, Stuart Davies⁶⁸, Nallaret Davila Cardozo⁶⁹, Thales de
472 Haulleville^{12,48}, Marcelo Brilhante de Medeiros⁷⁰, Jhon del Aguila Pasquel⁷¹, Géraldine Derroire⁷², Anthony
473 Di Fiore⁷³, Jean-Louis Doucet⁷⁴, Aurélie Dourdain⁷², Vincent Droissant⁷⁵, Luisa Fernanda Duque⁷⁶, Romeo
474 Ekoungoulou⁷⁷, Fernando Elias⁷⁸, Terry Erwin⁷⁹, Adriane Esquivel-Muelbert⁸⁰, Sophie Fauset⁸¹, Joice
475 Ferreira⁸², Gerardo Flores Llampazo⁸³, Ernest Foli⁸⁴, Andrew Ford⁵¹, Martin Gilpin¹, Jefferson S. Hall⁸⁵,
476 Keith C. Hamer⁸⁶, Alan C. Hamilton⁸⁷, David J. Harris⁸⁸, Terese B. Hart^{89,90}, Radim Hédí^{91,92}, Bruno
477 Herault⁷², Rafael Herrera⁹³, Niro Higuchi⁶, Annette Hladik⁹⁴, Eurídice Honorio Coronado⁷¹, Isau
478 Huamantupa-Chuquimaco⁹⁵, Walter Huaraca Huasco⁹⁵, Kathryn J. Jeffery⁹⁶, Eliana Jimenez-Rojas⁹⁷,
479 Michelle Kalamandeen¹, Marie-Noel Kamdem^{11,13,17,98}, Elizabeth Kearsley⁹⁹, Ricardo Keichi Umetsu¹⁰⁰, Lip
480 Khoon Kho Khoon¹⁰¹, Timothy Killeen¹⁰², Kanehiro Kitayama¹⁰³, Bente Klitgaard¹⁰⁴, Alexander Koch¹⁰⁵,
481 Nicolas Labrière⁵⁸, William Laurance¹⁰⁶, Susan Laurance¹⁰⁶, Miguel E. Leal¹⁰⁷, Aurora Levesley¹, Adriano
482 J. N. Lima⁶, Janvier Lisingo¹¹, Aline P. Lopes^{108,109}, Gabriela Lopez-Gonzalez¹, Tom Lovejoy¹¹⁰, Jon
483 Lovett¹, Richard Lowe¹¹¹, William E. Magnusson¹¹², Jagoba Malumbres-Olarte^{113,114}, Ângelo Gilberto
484 Manzatto¹¹⁵, Ben Hur Marimon Junior¹¹⁶, Andrew R. Marshall^{8,117,118}, Toby Marthews¹¹⁹, Simone Matias de
485 Almeida Reis^{14,19}, Colin Maycock¹²⁰, Karina Melgaço¹, Casimiro Mendoza¹²¹, Faizah Metali¹²², Vianet
486 Mihindou^{123,124}, William Milliken¹⁰⁴, Edward Mitchard¹²⁵, Paulo S. Morandi¹⁴, Hannah L. Mossman², Laszlo
487 Nagy¹²⁶, Henrique Nascimento⁶, David Neill¹²⁷, Reuben Nilus¹²⁸, Percy Núñez Vargas⁹⁵, Walter Palacios¹²⁹,
488 Nadir Pallqui Camacho^{1,95}, Julie Peacock¹, Colin Pendry¹³⁰, Maria Cristina Peñuela Mora¹³¹, Georgia C.
489 Pickavance¹, John Pipoly¹³², Nigel Pitman¹³³, Maureen Playfair¹³⁴, Lourens Poorter¹³⁵, John R. Poulsen²⁵,
490 Axel D. Poulsen¹³⁶, Richard Preziosi², Adriana Prieto¹³⁷, Richard Primack¹³⁸, Hirma Ramírez-Angulo¹³⁹, Jan
491 Reitsma¹⁴⁰, Maxime Réjou-Méchain⁷⁵, Zorayda Restrepo Correa¹⁴¹, Thaianie Rodrigues de Sousa⁶, Lily
492 Rodriguez Bayona¹⁴², Anand Roopsind¹⁴³, Agustín Rudas¹³⁷, Ervan Rutishauser^{42,144}, Kamariah Abu
493 Salim¹²², Rafael P. Salomão^{145,146}, Juliana Schiatti⁶, Douglas Sheil¹⁴⁷, Richarlly C. Silva^{57,148}, Javier Silva
494 Espejo¹⁴⁹, Camila Silva Valeria³⁸, Marcos Silveira⁵⁷, Murielle Simo-Droissart¹⁷, Marcelo Fragomeni
495 Simon⁷⁰, James Singh¹⁵⁰, Yahn Carlos Soto Shareva¹⁵, Clement Stahl⁵⁴, Juliana Stropp¹⁵¹, Rahayu Sukri¹²²,
496 Terry Sunderland^{152,153}, Martin Svátek¹⁵⁴, Michael D. Swaine¹⁵⁵, Varun Swamy¹⁵⁶, Hermann Taedoumg¹⁷,
497 Joey Talbot¹, James Taplin¹⁵⁷, David Taylor¹⁵⁸, Hans ter Steege^{159,160}, John Terborgh²⁵, Raquel Thomas¹⁴³,
498 Sean C. Thomas¹⁶¹, Armando Torres-Lezama¹⁶², Peter Umunay^{163,164}, Luis Valenzuela Gamarra¹⁵, Geertje
499 van der Heijden¹⁶⁵, Peter van der Hout¹⁶⁶, Peter van der Meer¹⁶⁷, Mark van Nieuwstadt¹⁶⁸, Hans Verbeek⁹⁹,
500 Ronald Vernimmen¹⁶⁹, Alberto Vicentini⁶, Ima Célia Guimarães Vieira¹⁴⁶, Emilio Vilanova Torre¹⁷⁰, Jason
501 Vleminckx³⁶, Vincent Vos¹⁷², Ophelia Wang¹⁷³, Lee J. T. White^{124,174,175}, Simon Willcock¹⁷⁶, John T.
502 Woods¹⁷⁷, Verginia Wortel¹⁷⁸, Kenneth Young¹⁷⁹, Roderick Zagt¹⁸⁰, Lise Zemagho¹⁷, Pieter A. Zuidema⁵⁰,
503 Joeri A. Zwarts^{178,181}, Oliver L. Phillips¹

504

505 **This file includes:**
506 Materials and Methods
507 Figures S1 – S15
508 Tables S1 – S2
509

510 **Materials and Methods**

511 Forest census data

512 Our plots come from the RAINFOR, AfriTRON, and T-FORCES networks. Forest inventory plots
513 were located in lowland (<1200 m), old-growth, closed-canopy forests that were not known to have
514 been subject to anthropogenic disturbance through fire or selective logging. Plots characterised
515 floristically as dry forest were not included, as were plots that received less than 1200 mm
516 precipitation each year. We also did not include plots in white sand, swamp and seasonally flooded
517 forests, as we expect these to experience marked edaphic constraints (extreme nutrient limitation for
518 white sand forests (32), stress caused by hypoxic conditions for swamp and seasonally flooded forests
519 (33)). All plots were ≥ 0.2 ha (median size = 1 ha) and were monitored for at least two years (median
520 monitoring period = 9.7 years). All censuses were prior to the 2015-16 very strong El Niño event, as
521 we expected that event to suppress carbon gains relative to the long-term mean.

522 Forest inventory plots were sampled using standardised protocols (34), where all live stems with
523 diameter ≥ 100 mm were measured at 1.3 m or 50 cm above buttresses and deformities. Trees were
524 tagged so that the same tree could be identified in subsequent censuses. In some cases the point of
525 diameter measurement (POM) had to be moved due to upward growth of buttresses and deformities.
526 For these trees we use the D_{mean} approach from Talbot et al. (35).

527 In a few cases (6 plots) the minimum diameter measured changed over time, or palms and
528 *Phenakospermum* were excluded in some censuses. For these, we estimated aboveground biomass
529 (AGB, subsequently converted to carbon stocks) and aboveground woody production (AGWP,
530 subsequently converted to carbon gains) using a minimum diameter or taxonomic protocol that could
531 be consistently applied across censuses, and scaled these values by the aboveground biomass ratio
532 between that protocol and all stems ≥ 100 mm protocol for censuses when all stems were measured.
533 Some plots had nested designs where the plot was split into subplots with different minimum diameter
534 protocols (69 plots). For these, we only analysed the area conforming to our minimum diameter
535 protocol. For analysis, we grouped small (≤ 0.5 ha) plots within 1 km of each other, and also grouped
536 contiguous larger plots (18 plots), as these will experience equivalent climate and larger plots are less
537 sensitive to stochastic tree fall events (36).

538 Data were curated in ForestPlots.net (37, 38), or were subject to equivalent offline handling, and
539 experienced the same quality control procedures. Details of quality control procedures are described
540 in Brienen et al. (39). Our final dataset consists of 590 sampling units (hereafter plots) covering 637.2
541 ha, with 2.2 million measurements of 670,499 unique stems. For validating models of carbon stocks
542 an additional dataset of 223 single-census plots using the same measurement protocols was assembled
543 from the same networks (see section “Validation with independent single-census plot dataset” below).

544

545 Estimating above-ground biomass

546 Diameter measurements were converted to estimates of aboveground biomass (AGB). For dicot trees
547 we used the allometric equation

$$548 \text{ AGB} = 0.673 \times (\rho D^2 H)^{0.976}, \quad [1]$$

549 from Chave et al. (40), where ρ is wood density (from (41, 42)) and H is tree height estimated using
550 allometric equations described below. For monocots and tree ferns, we used a palm-specific
551 allometric equation

$$552 \ln(\text{AGB}) = -3.3488 + 2.7483 \cdot \ln(D), \quad [2]$$

553 from Goodman et al. (43), where D is the measured diameter.

554 The heights of a subset of trees in our dataset were measured in the field, either with a laser
555 rangefinder, hypsometer, or clinometer, or directly by climbing the tree. We filtered this dataset to
556 stems with measured diameters, height ≤ 90 m, diameters ≥ 90 mm DBH, as height-diameter
557 allometries of saplings differ from those of more mature trees, and to stems that were not broken,
558 leaning or fallen. This gave a total of 78,899 height measurements. We used this dataset to fit local
559 height-diameter allometric models, as these refine AGB estimates by capturing spatial variation in
560 height-diameter allometries missed by large-scale allometric models (44). Height data were not
561 available from every plot, so to ensure consistent treatment of plots height-diameter models were
562 constructed for each biogeographic region. We fitted three parameter asymptotic models (45) of the
563 form

$$564 H = a(1 - \exp(-bD^c)), \quad [3]$$

565 where a, b and c are estimated parameters ('Weibull' models, 46). We fitted these models either
566 treating each observation equally or with case weights proportional to each trees' basal area. These
567 weights give more importance to large trees during model fitting. We selected the best fitting of these
568 models, determining this as the model that minimised prediction error of stand biomass when
569 calculated with estimated heights or observed heights (44). Weibull models were implemented using
570 the nls function in R with default settings. Starting values of $a = 25$, $b = 0.05$ and $c = 0.7$ were chosen
571 following trial and error as they led to regular model convergence. Where models did not converge
572 this was usually because the height-diameter relationship did not reach an asymptote, so in these cases
573 we used the log-log model $\ln(H) = a + b(\ln(D))$ to estimate height, where b gives the scaling exponent
574 of a power law relationship between height and diameter. We checked if models gave unrealistic
575 predictions by applying models to predict the height of all trees in the biogeographic region, and

576 excluded models that predicted any tree height 10 % higher than the tallest tree we recorded in that
577 continent.

578

579 Estimating above-ground woody production

580 We estimated AGWP following Talbot et al. (35). AGWP is comprised of four components, (1) the
581 sum of growth of surviving trees, (2) the sum of AGB of new recruits, (3) the sum of unobserved
582 growth of trees that died during a census interval and (4) the sum of growth of unobserved recruits
583 that entered then died during a census interval. Accounting for the latter two components is necessary
584 to avoid census-interval length effects, as more AGWP in these components will be missed due to the
585 greater mortality of trees that accumulates over longer census intervals.

586 Components 3 and 4 can be estimated using two quantities that can be calculated from observed stem-
587 dynamics in each plot; per-area annual recruitment (R_a) and per-capita annual mortality (m_a). Per-
588 capita mortality is calculated from the ratio of surviving stems to initial stems, using equation 5 in
589 Kohyama et al. (47). Per-area annual recruitment is calculated using estimated mortality rates and the
590 observed change in the number of stems over a census interval, using equation 11 of Kohyama et al.
591 (47).

592 To estimate the unobserved growth of stems that died during a census interval, we first use plot-level
593 per-capita mortality rates (m_a) to estimate how many trees are expected to have died in each year of
594 the census interval, and from that calculate the mean number of years that trees that died during the
595 census interval would have lived before death. The diameter of tree at death (D_{death}) can then be
596 estimated as

$$597 \quad D_{\text{death}} = D_{\text{start}} \times G \times Y_{\text{mean}} \quad [4]$$

598 where D_{start} is the diameter at the start of the census interval, G is the plot-level median growth rate of
599 the size class the tree was in at the start of the census interval (size classes are defined as $D < 200$ mm,
600 $400 \text{ mm} > D \geq 200$ mm, and $D \geq 400$ mm) and Y_{mean} is the mean number of years trees survived in
601 the census interval before dying. The diameter at death is then converted to AGB at death using
602 allometric equations (equation 1, except for ferns and monocots where equation 2 is used), and the
603 unobserved growth is calculated as the difference between AGB at death and AGB at the start of the
604 census.

605 To estimate the growth of recruits that were not observed because they died during the census
606 interval, we first need to estimate the number of unobserved recruits. This can be estimated from per-
607 area annual recruitment (R_a) and per-capita annual mortality (m_a): R_a gives the number of stems per ha
608 that recruit in a given year, and the probability of each recruit surviving until the next census (P_{surv}) is

609 $P_{\text{surv}} = (1 - m_a)^T$, where T is the number of years remaining in the census interval. The number of
610 recruits in a given year that survive to the next census is $R_a - P_{\text{surv}}R_a$. Summing this for each year in a
611 census interval gives the total number of unobserved recruits in that census interval. We then need to
612 estimate how long each recruit was alive for. From m_a we can calculate the number of recruits in a
613 given year that died in each subsequent year, and from this calculate the mean life-span of recruits in a
614 given year that died before the next census. The average life-span of unobserved recruits ($Y_{\text{mean-rec}}$) is
615 the weighted mean of each cohort's lifespan, weighted by the number of unobserved recruits in each
616 year. Diameter at death is given in mm by

$$617 \quad D_{\text{death}} = 100 + (G \times Y_{\text{mean-rec}}) \quad [5]$$

618 where G is the plot-level median growth rate of the smallest size class (i.e. $D < 200$ mm).
619 Aboveground biomass of recruits at the time of death is estimated using equation 1. These corrections
620 for unobserved growth have a marginal impact on AGWP calculations, collectively accounting on
621 average for just 2.3 % of estimated plot-level AGWP.

622 AGB was calculated for each census, and AGWP was calculated for each census interval, and the
623 time-weighted mean of each was taken to give one value per plot. We used a time-weighted mean to
624 give greater importance to AGB estimates separated by longer census-intervals, as these will be more
625 independent. Estimates of AGB and AGWP were converted to carbon stocks and carbon gains by
626 multiplying by 0.456 (48). Carbon residence time was then estimated as carbon stocks /carbon gains,
627 and represents the length of time carbon resides in living biomass before being passed to the litter and
628 necromass pools (49). Calculations to estimate AGB and AGWP were performed using the R package
629 BiomasaFP (50).

630

631 Obtaining environmental data

632 Most climate data were obtained from climate data from Worldclim2 (51) as it provides the highest
633 resolution (~ 1 km) pantropical climate data, although we note that some regions, such as central
634 Africa, have limited station data. We extracted monthly data for the following variables: mean daily
635 minimum temperature, mean daily maximum temperature, precipitation, solar radiation and wind
636 speed, In addition to calculating the standard series of 19 bioclimatic variables, using the dismo R
637 package (52), we calculated 1) mean daily maximum temperature, $BIO1 + BIO2/2$, 2) mean daily
638 minimum temperature, $BIO1 - BIO2/2$, 3) maximum cumulative water deficit as the minimum across
639 the year of monthly cumulative water deficit W,

$$640 \quad W_i = W_{i-1} - \min(0, P_i - 100) , \quad [6]$$

641 where P is monthly precipitation in mm, and 100 represents measured evapotranspiration. This
642 calculation was run for a year from the wettest month in the year, starting at a water deficit of zero, 4)
643 the number of months where monthly cumulative water deficit was negative, 5) the number of months
644 where monthly precipitation was below 100 mm (i.e. less than evapotranspiration), 6) mean annual
645 solar radiation, 7) mean annual wind speed, and 8) vapour pressure deficit ($VPD = SVP - \text{vapour}$
646 pressure , where saturated vapour pressure, $SVP, = 0.611 \times e^{(17.502 \text{ temperature}) / (\text{temperature} + 240.97)}$). We also
647 obtained data on cloud frequency at ~1 km resolution from Wilson & Jetz (53), who processed twice-
648 daily MODIS satellite images. Temperature values were adjusted for differences in altitude between
649 the plot and the 1 km grid cell used for Worldclim interpolation, as these can differ in topographically
650 diverse regions, using lapse rates, so that $T_{\text{plot}} = T_{\text{worldclim}} + 0.005 \times (A_{\text{worldclim}} - A_{\text{plot}})$, where T is
651 temperature (°C) and A is altitude (m). Temperature values were also corrected for systematic
652 warming trends. To do this, the mean annual temperature in each grid-cell in each year was extracted
653 from the CRU TS 3.24 dataset (54), and robust linear regression used to estimate grid-cell specific
654 warming rates. These were used to adjust Worldclim2 temperature values for the difference between
655 the midpoint of plot monitoring and the midpoint of the Worldclim2 climatology.

656 Data on soil texture and chemistry was obtained at 1 km resolution from the SoilGrids dataset (55),
657 with this resolution selected to match the resolution of the climate data. From this we extracted CEC,
658 representing soil fertility, and percentage clay, representing soil texture. For each soil variable we
659 calculated the depth-weighted average for 0 – 30 cm.

660 Statistical analysis

661 We used linear models to relate carbon, carbon gains and carbon residence time to environmental
662 explanatory variables. The role of different explanatory variables was assessed using multi-model
663 inference.

664 Response variables were positively skewed and had positive mean-variance relationships, so were
665 log-transformed to meet the assumption of normality and reduce heterogeneity in variances. The log-
666 normal nature of forest carbon stocks and dynamics means that there is greater potential for variation
667 when forests are large, which could be due to the non-linear scaling of tree biomass and tree basal
668 area.

669 We selected explanatory variables to represent hypothesised ways in which climate could affect
670 carbon stocks (Table S1). We assessed collinearity within this set of explanatory variables using
671 variance inflation factors (VIF) and pairwise correlations. Because of collinearity, we had to exclude
672 VPD, total precipitation, use only one of MCWD and precipitation in the driest quarter, and could
673 include both minimum and maximum temperature but not mean annual temperature. We used
674 precipitation in the driest quarter rather than MCWD as the latter is zero truncated and so is less
675 amenable to regression analysis. After removing these variables all pairwise correlations (including

676 with soil explanatory variables) were weak enough not to cause problems through collinearity ($r < 0.6$
677 and $VIF < 3$).

678 To account for variation other than in climate we also included soil variables relating to texture (%
679 clay) and fertility (CEC), and included continent specific intercepts to account for biogeographic
680 variation in carbon. To account for unmeasured environmental gradients (e.g. soil variation not
681 captured by the SoilGrids variables), we used Moran's eigenvector maps as explanatory variables,
682 selecting eigenvectors the corresponded to positive spatial autocorrelation in the distance matrix (56).
683 These variables act as a proxy for unmeasured spatial gradients by capturing positive spatial
684 associations between plots.

685 Plots differed in their area and the length of time they were monitored for. This is likely to affect the
686 variance of carbon stocks, carbon gains and carbon residence time, as smaller plots or plots only
687 monitored for short periods are more likely to be sensitive to the mortality of a few large trees. To
688 account for this, we used case weights relating to plot area and monitoring period. Following Lewis et
689 al. (57), we selected weights by relating residuals from our linear models to plot area and to plot
690 monitoring period, and subsequently assessing which root transformation of plot area/ monitoring
691 period removed the pattern in the residuals when used as a weight. Selected weights were: carbon
692 stocks, $\text{Area}^{1/3}$; carbon gains, $\text{Monitoring length}^{1/7}$; carbon residence time, $\text{Area}^{1/9} + \text{Monitoring}$
693 $\text{length}^{1/12} - 1$.

694 We fitted all subsets of the general linear model with explanatory variables described above, forcing
695 spatial eigenvectors into all models. We then averaged the subset of models where $\Delta \text{AIC} < 4$, using
696 full averaging so variables that do not appear in the model get the value of zero for their coefficients.
697 This means that model averaged coefficients of terms with limited support exhibit shrinkage towards
698 zero. Multi-model inference was performed using the MuMIn R package (58).

699 We assessed whether the two climate variables found to have important additive effects on carbon
700 stocks in this analysis (mean daily maximum temperature in the warmest month and precipitation in
701 the driest quarter) interacted with each other by adding an interaction term between these variables to
702 the full generalised linear model of carbon stocks as a function of other climate and soil variables,
703 continent and spatial eigenvectors. We compared these two models using AIC. We repeated this with
704 carbon gains and carbon residence time as response variables.

705 To assess whether the temperature carbon relationship was non-linear we used breakpoint regression
706 implemented in the segmented R package (59). This estimates a breakpoint in the explanatory variable
707 at which the slope of the relationship with the response variable changes. We estimated the breakpoint
708 for the mean daily maximum temperature in the warmest month variable in the full model with a
709 temperature-precipitation interaction described above. We assessed the support for the breakpoint by

710 comparing the AIC of the model with a breakpoint with the AIC of a model with a linear relationship.
711 We repeated this with carbon gains and carbon residence time as response variables.

712 We also analysed spatial variation in carbon stocks as a function of the above climate and soil
713 variables and spatial eigenvectors using Random Forest decision tree algorithms (22) implemented
714 using the randomForest R package (60). We assessed variable importance by calculating the average
715 increase in node purity across all decision trees (measured by residual sum of squares) when using the
716 variable to split the data. We assessed modelled relationships between response and explanatory
717 variables using partial plots, which show predicted change in the response variable, averaged across
718 trees, when changing the explanatory variable and holding all other variables constant.

719 To compliment this analysis based on relationships expected a priori, we also performed an
720 exploratory analysis to assess whether other climate variables excluded from the full general linear
721 models had an effect on carbon. To do this, we fitted linear models to assess the bivariate relationship
722 of carbon with each climate variable, with continent also included as an explanatory variable to
723 account for biogeographic variation in forest characteristics.

724

725 Validation with independent single-census plot dataset

726 We assessed whether the relationships with environmental variables identified in the analyses of
727 multi-census plot data described above held when applied to an additional dataset of 223 single-
728 census plots. As the single-census data were not used in any of the analyses above they did not
729 influence modelling decisions, so provide an independent test of the relationships identified with the
730 multi-census plot analysis.

731 Single-census plots were extracted from the ForestPlots.net database (37, 38) using the same plot-
732 selection criteria as for the multi-census plots, except that censuses during or following the 2015-16
733 strong El Niño were included in the single-census plot dataset as we expected that carbon stocks,
734 unlike gains, would still remain close to their long-term mean.

735 We fitted a general linear model with the five climate explanatory variables, soil fertility and texture,
736 continent and spatial eigenvector, and model averaging of all subsets of this model as described for
737 the multi-census plots. We performed this analysis using just the single-census plots and a combined
738 dataset of single and multi-census plots.

739

740

741

742 Scaling results to the biome

743 We applied the non-linear relationship between carbon stocks and mean daily maximum temperature
744 in the warmest month identified by the breakpoint regression to estimate the total change in carbon
745 stock due to temperature effects alone for different scenarios of temperature increase. We delimited
746 the biome extent using the WWF tropical and subtropical moist broadleaved forest biome (61),
747 restricted to tropical latitudes, and further refined it by excluding grid-cells with $< 50 \text{ Mg C ha}^{-1}$ using
748 data from (30), as these are unlikely to be forest. Calculations were conducted at 10-minute
749 resolution. The non-linear relationship between temperature and carbon means that the change in
750 biomass for a given increase in temperature will depend on the baseline temperature. For each grid-
751 cell we predicted the percentage change in carbon for a given temperature increase from the baseline
752 temperature in that grid-cell based on the non-linear relationship identified in our statistical model,
753 holding all other variables constant. We then used a reference carbon stock map (30) to convert
754 percentage change to change in carbon stocks per hectare (in Mg ha^{-1}). To calculate change in carbon
755 stocks for the whole grid-cell, we multiplied change per hectare by the area of the grid-cell in
756 hectares, and then adjusted this by the proportion of the grid-cell that was forested by multiplying by
757 2014 forest cover (62). Total change for the biome (in Pg) was calculated by summing these grid-cell
758 level values. Uncertainty due to our statistical model was assessed by generating multiple predictions
759 by resampling model parameters (breakpoint threshold, slope below breakpoint, slope above
760 breakpoint), and extracting quantiles from the resultant distribution of predicted change values.
761 Aboveground biomass carbon values were scaled to include root biomass based on a root to shoot
762 ratio of 0.19 in tropical evergreen forests (63).

763 The Avitabile et al (30) aboveground biomass map was chosen to provide reference carbon stocks.
764 While other maps have previously been produced by Saatchi et al. (64) and Baccini et al. (65) we
765 selected the Avitabile map because it synthesises the earlier maps (see Mitchard et al. (66) for
766 discussion of substantial differences between these maps) and is anchored by more field data.
767 Importantly, the Avitabile map reproduces spatial patterns in aboveground biomass that have been
768 described from field data but are absent in the Saatchi or Baccini maps, including the much higher
769 biomass density of north-east Amazonian forests due to tall trees and very high wood density (67).
770 Nevertheless, we also investigated the consequences of using the Saatchi or Baccini maps for our
771 estimates of biomewide thermal sensitivity and spatial patterns of change in carbon stocks (Fig S15).

772 We investigated three temperature change scenarios. Firstly, we applied a 1°C increase to all
773 locations. Secondly, we assessed the consequence of global temperatures stabilizing 1.5°C above pre-
774 industrial levels for the equilibrium temperature response of tropical forest carbon. Finally, we
775 assessed the consequence of global temperatures stabilizing 2°C above pre-industrial levels. For the
776 latter two we obtained data from CMIP5 climate models, using downscaled future climate projections

777 based on the Worldclim climatology (68). As downscaling was performed using Worldclim version
 778 1.4 (69) and our statistical models use Worldclim version 2, we calculated the warming anomaly in
 779 each grid-cell from the current Worldclim version 1.4 conditions, and applied this to the Worldclim 2
 780 data to obtain future temperature. RCP scenarios and time-points were chosen to give global
 781 temperature increases that best match 1.5°C and 2°C above pre-industrial. Importantly, these future
 782 climate projections were used to capture the spatially varying nature of warming, and our predictions
 783 relate to the long-term response of vegetation if the climate stabilised at these new warming levels,
 784 rather than being predictions of transient responses at these specific time-points. For 1.5°C we used
 785 RCP 2.6 averaged for 2040-2060 (median temperature increase across models = 1.5°C, (70)). For
 786 2°C, we used RCP 2.6 averaged for 2040-2060 (median temperature increase models = 1.9°C (70)).
 787 Note that predicted increases in maximum temperatures were often considerably greater than the
 788 global increase, especially in South America. For both scenarios we used the median predicted
 789 temperature change for each grid-cell from an ensemble of 15 models (BCC-CSM1-1, CCSM4,
 790 CNRM-CM5, GFDL-CM3, GFDL-ESM2G, GISS-E2-R, HadGEM2-AO, HadGEM-ES, IPSL-
 791 CM5A-LR, MIROC-ESM-CHEM, MIROC-ESM, MIROC5, MPI-ESM-LR, MRI-CGCM3,
 792 NorESM1-M).

793 We assessed the potential for long-term carbon dioxide growth stimulation to offset these long-term
 794 temperature effects. We used CO₂ concentrations from the RCP scenarios and time-points described
 795 above, which approximate the long-term concentrations if the climate stabilised at the new
 796 temperatures (71). Thus the 1.5°C and 2°C scenarios were associated with CO₂ concentrations of 443
 797 ppm and 487 ppm respectively (72). We cannot assess the effect of CO₂ on biomass from our spatial
 798 dataset, so instead used independent estimates of CO₂ effects from other sources. Firstly, we obtained
 799 CO₂ only effects on net primary production (NPP) extracted from an ensemble of CMIP5 earth system
 800 models by (73). This gives the proportional change in NPP for evergreen forests (note that this also
 801 includes boreal forests) over 1980-2010, standardised to a 100 ppm increase in CO₂ concentration. To
 802 propagate this through to changes in AGB under future CO₂ conditions we first estimated the
 803 logarithmic dependency of NPP on CO₂ (74) by substituting values of NPP and CO₂ at time zero and t
 804 (from (73)) into the equation,

$$805 \quad NPP_t = NPP_0 \left[1 + \beta \ln \left(\frac{[CO_2]_t}{[CO_2]_0} \right) \right] \quad \text{Equation 7}$$

806 This equation can be used to compute NPP annually given an initial NPP estimate and a time series of
 807 atmospheric CO₂ concentrations (from a combination of the observed record from pre-industrial and
 808 the RCP 4.5 scenario, modified so that it stabilises at 487 or 443 ppm depending on warming
 809 scenario). Initial pre-industrial NPP was back-calculated from present-day values using Equation 7,
 810 with 13.3 Mg C ha⁻¹ yr⁻¹ (mean of nine Amazon plots where NPP has been measured, from (75)) used

811 for present-day NPP. To propagate NPP into change in woody biomass (following (49)) we used the
812 equation

$$813 \quad \frac{dM_{\text{wood}}}{dt} = \alpha_{\text{wood}} N_{\text{P}} - \frac{M_{\text{wood}}}{\tau_{\text{wood}}} \quad \text{Equation 8}$$

814 where M_{wood} is woody biomass, N_{p} is NPP, α_{wood} is the allocation of NPP to wood (taken as 0.33, the
815 mean value across nine plots from (75)) and τ_{wood} is the residence time of woody biomass, taken as
816 59.1 years (the median value across plots used in this study). This model (equations 7 and 8) was run
817 from pre-industrial to 2500, enabling us to see the equilibrium effect of increased CO_2 concentrations
818 on biomass, assuming temporally invariant allocation and residence time. We calculated the
819 proportional change in biomass from 2000 to 2500, and applied this to the reference carbon stock map
820 to obtain predicted equilibrium change in aboveground biomass due to CO_2 effects.

821 The effects of CO_2 in earth system models have been reported to be larger than those deduced from
822 satellite data or CO_2 enrichment experiments (73), so we also ran the above model using changes in
823 NPP reported from a synthesis of free-air CO_2 enrichment experiments conducted in forests (73).
824 Finally, we looked at the impact of using CO_2 effects derived from a recent large meta-analysis of
825 CO_2 enrichment experiments (76), which reported a 12.5 % increase in biomass of tropical trees for a
826 250 ppm increase in CO_2 concentration. As this relationship was reported to be linear (76) we used
827 linear interpolation to estimate the change in biomass under CO_2 concentrations associated with each
828 warming scenario (i.e. 443 and 487 ppm). To estimate long-term changes in biomass accounting for
829 both temperature and carbon dioxide, we first applied the CO_2 relationship to estimate the change in
830 biomass due to carbon dioxide growth stimulation, and then assessed the effects of warmer
831 temperatures from this revised baseline. Our approach allows a simple assessment of CO_2 effects
832 exploring a range of different effect strengths. Real-world responses will likely be more complex,
833 with, for example, nutrient limitation potentially affecting the extent to which growth is stimulated by
834 CO_2 (76).

835 Temperature sensitivity of CMIP5 models

836 The temperature sensitivity (γ_{LT}) of coupled climate carbon cycle models can be identified by
837 comparing responses of carbon stocks in coupled and uncoupled simulations forced with a 1%
838 increase in CO_2 concentrations per year (respectively, these are the 1pctCO2 and esmFixClim
839 simulations), following Wenzel et al. (77). Both coupled and uncoupled simulations are exposed to
840 the same increase in CO_2 concentration, but in the uncoupled simulation temperature is not directly
841 affected by this increase in CO_2 .

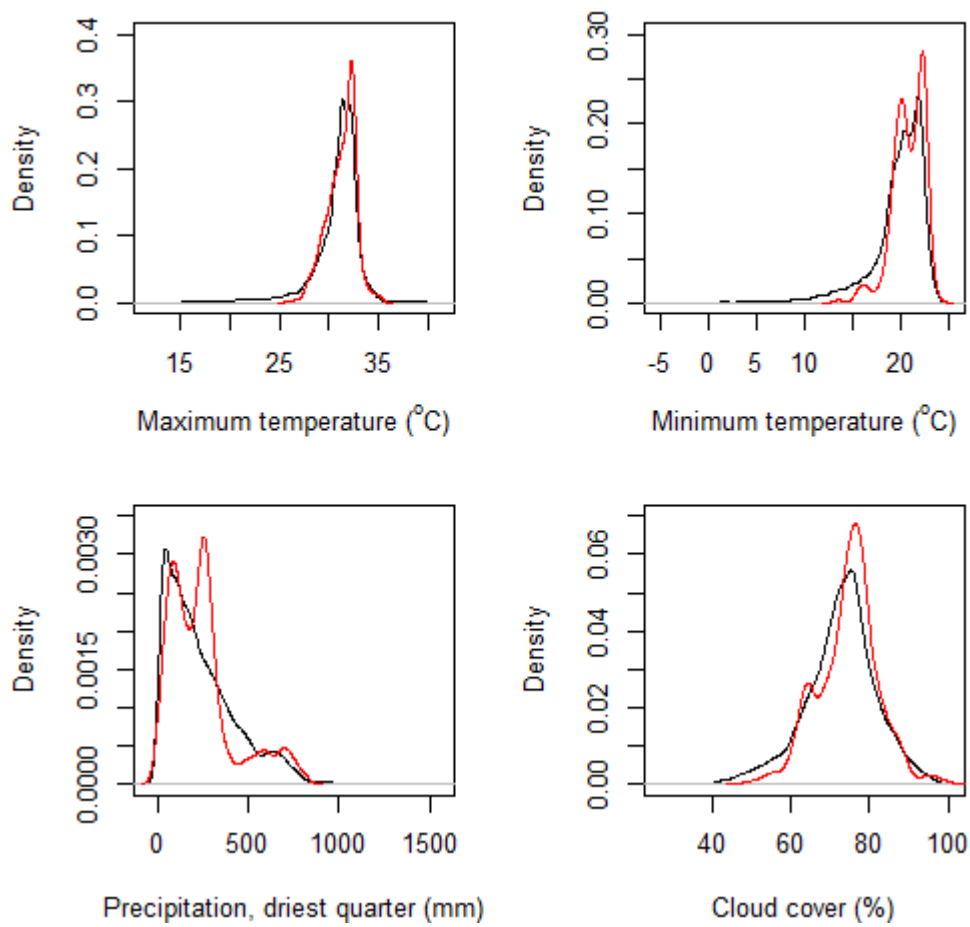
842 Vegetation carbon outputs are reported from six CMIP5 models, each with coupled and uncoupled
843 simulations (78, 79). For all simulations, we calculated the change in vegetation carbon (the cVeg

844 variable) in the tropics between year 110 and year 30 of the experiment, and also calculated the
845 difference in land temperature (the t_{as} variable). The change in vegetation carbon due to temperature
846 alone was calculated by taking the difference in change in vegetation carbon in the coupled (ΔC_{vegC})
847 and uncoupled (ΔC_{vegU}) simulation, and this was then divided by the change in tropical land
848 temperature (ΔT) to obtain the temperature sensitivity of the model,

$$849 \quad \gamma_{LT} = (\Delta C_{vegC} - \Delta C_{vegU}) / \Delta T \quad \text{Equation 9.}$$

850 We calculated the temperature sensitivity of the six CMIP5 models that report vegetation carbon:
851 CESM-1-BGC ($\gamma_{LT} = -0.7 \text{ Pg C } ^\circ\text{C}^{-1}$), GFDL-ESM2M ($\gamma_{LT} = -58.4 \text{ Pg C } ^\circ\text{C}^{-1}$), HadGEM2-ES ($\gamma_{LT} = -$
852 $9.2 \text{ Pg C } ^\circ\text{C}^{-1}$), IPSL-CM5A-LR ($\gamma_{LT} = -11.3 \text{ Pg C } ^\circ\text{C}^{-1}$), MPI-ESM-LR ($\gamma_{LT} = -22.8 \text{ Pg C } ^\circ\text{C}^{-1}$) and
853 NorESM1-ME ($\gamma_{LT} = -1.0 \text{ Pg C } ^\circ\text{C}^{-1}$). Note that the simulations do not run to equilibrium (77), so
854 changes in carbon stocks due to increased temperature may not be fully realised.

855

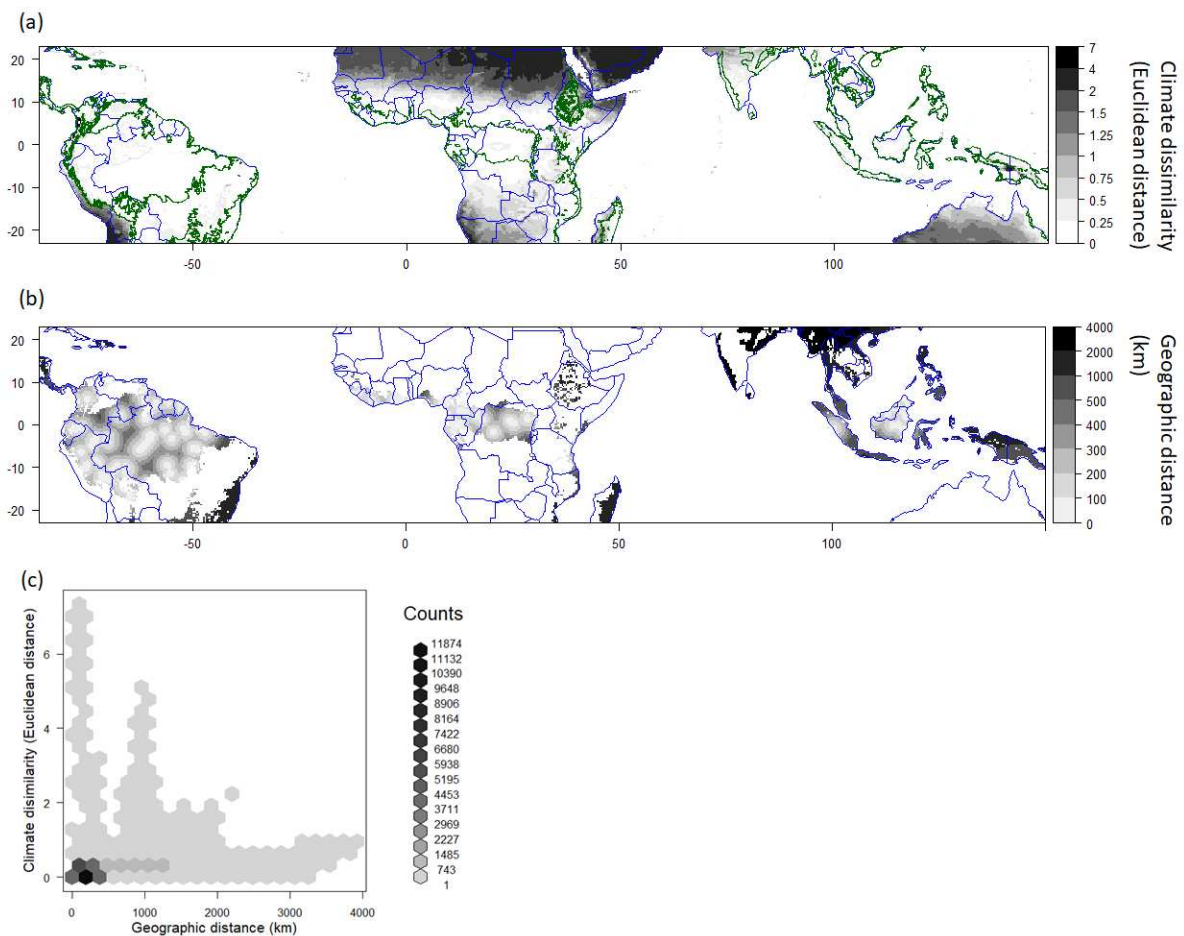


856

857 **Figure S1.** Climate space represented by our plot network. Red lines show the probability density
858 function of each variable in our multi-census plot network. Black lines show the probability density
859 across 10 minute grid-cells in the biome, restricted to areas with forest cover in GLC 2000 (80).

860

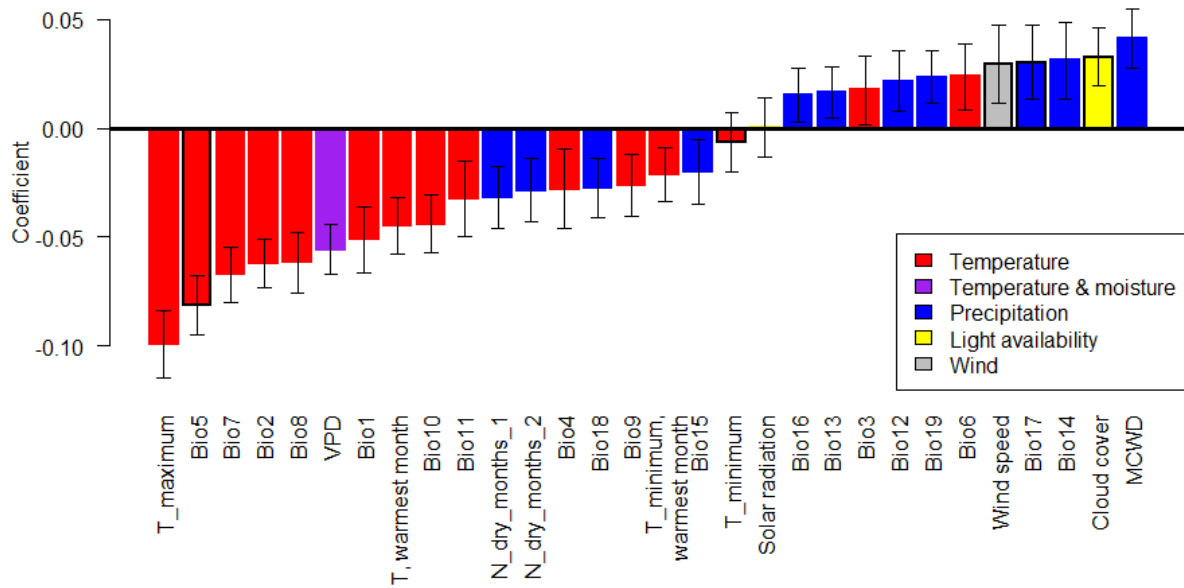
861



862

863 **Figure S2.** Ability of our plot network to represent the climate conditions found in the moist tropical
 864 forest biome. (a) Minimum climate dissimilarity (measured as Euclidean distance on variables scaled
 865 by their standard deviation). Climate variables used are the same as in Fig. 2) between 10 minute grid
 866 cells and the multi-census plot network. Green lines indicate the extent of the biome. (b) Geographic
 867 distance (km) between grid cells and the multi-census plot network. (c) Relationship between climatic
 868 and geographic distance of 10 minute grid cells across the tropical forest biome to our plot network.
 869 The lack of relationship between climate dissimilarity and geographical distance, alongside the mostly
 870 low climatic dissimilarities, shows that our sampling is sufficient to capture the environmental space
 871 of the biome and that we can reasonably extrapolate to geographically distant areas from our plots,
 872 which are in any case largely deforested already and hence contribute very little to our projected
 873 biome-wide carbon response to climate change. (These tropical moist forest areas that are poorly
 874 sampled and largely lost include the Atlantic Forests in Brazil, Andean Forests in western South
 875 America, eastern Caribbean, Madagascar, and much of tropical South Asia, south China, continental
 876 Southeast Asia, Philippines, Sumatra and Java).

877



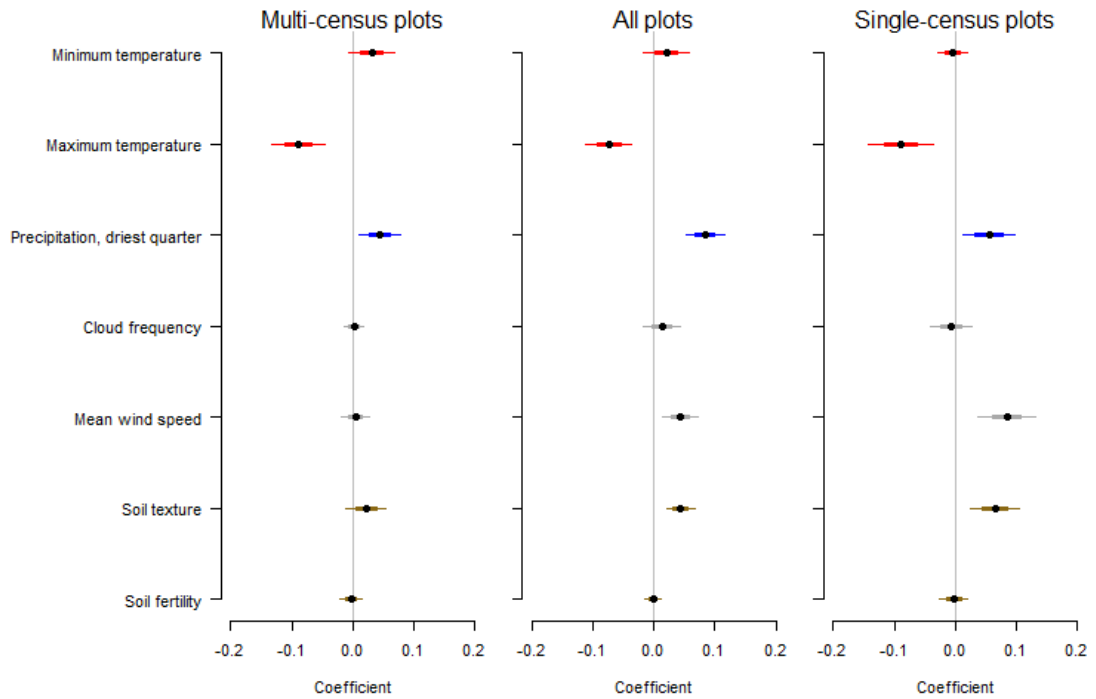
878

Figure S3. Relationships between individual climate variables and tropical forest aboveground carbon stocks. Standardised coefficients are from models with the climate variable and continent as explanatory variables and show change in $\ln(\text{carbon})$ for a standard deviation change in the explanatory variable. Error bars show standard errors. Variables used in the main analysis have black outlines. Full variable names are: T_maximum – mean daily maximum temperature, Bio5 – mean daily maximum temperature in the warmest month, Bio7 – annual temperature range, Bio2 – mean diurnal temperature range, Bio8 – mean temperature in the wettest quarter, VPD – vapour pressure deficit, Bio1 – mean annual temperature, Bio10 – mean temperature in the warmest quarter, Bio11 – mean temperature in the coldest quarter, N_dry_months_1 – number of months with negative cumulative water deficit, N_dry_months_2 – number of months where precipitation is less than evapotranspiration, Bio4 – temperature seasonality, Bio18 – precipitation in the warmest quarter, Bio9 – mean temperature in the driest quarter, T_minimum warmest month – mean daily minimum temperature in the warmest month, Bio15 – precipitation seasonality, T_minimum – mean daily minimum temperature, Bio16 – precipitation in the wettest quarter, Bio13 – precipitation in the wettest month, Bio3 – isothermality, Bio12 – annual precipitation, Bio19 – precipitation in the coldest quarter, Bio6 – mean daily minimum temperature in the coldest month, Wind speed – mean daily wind speed, Bio17 – precipitation in the driest quarter, Bio14 – precipitation in the driest month, Cloud cover – proportion of MODIS passes with cloud present, MCWD – maximum cumulative water deficit (note this is negative when water deficit is high, so a positive relationship with MCWD indicates higher carbon when water deficits are less).

899

900

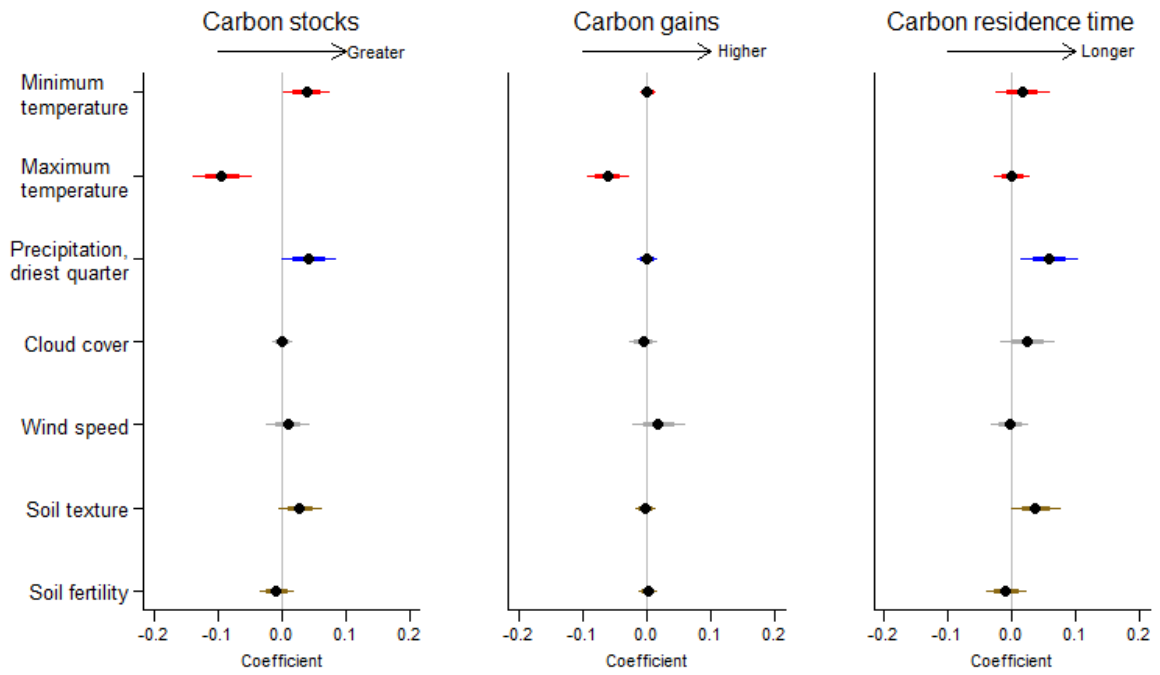
901



902

903 **Figure S4.** Validation of tropical forest carbon stock sensitivity model against an independent dataset
 904 of 223 single-census plots from our networks measured with the same protocols. Model-averaged
 905 shrinkage adjusted coefficients from multiple regression models of biomass carbon stocks as a
 906 function of climate, soil, biogeography and spatial eigenvectors. Models were either fitted to the
 907 multi-census plot dataset (as in Fig. 2), to the single-census plot dataset, or to the combined dataset.
 908 This analysis shows that the relationships identified to be most important in the main multi-census
 909 plot analysis (i.e. the negative relationship between carbon stocks and maximum temperature and
 910 positive relationship with precipitation in the driest quarter) are also found in an independent dataset,
 911 which was not used for preliminary analysis so did not influence the choice of explanatory variables.

912



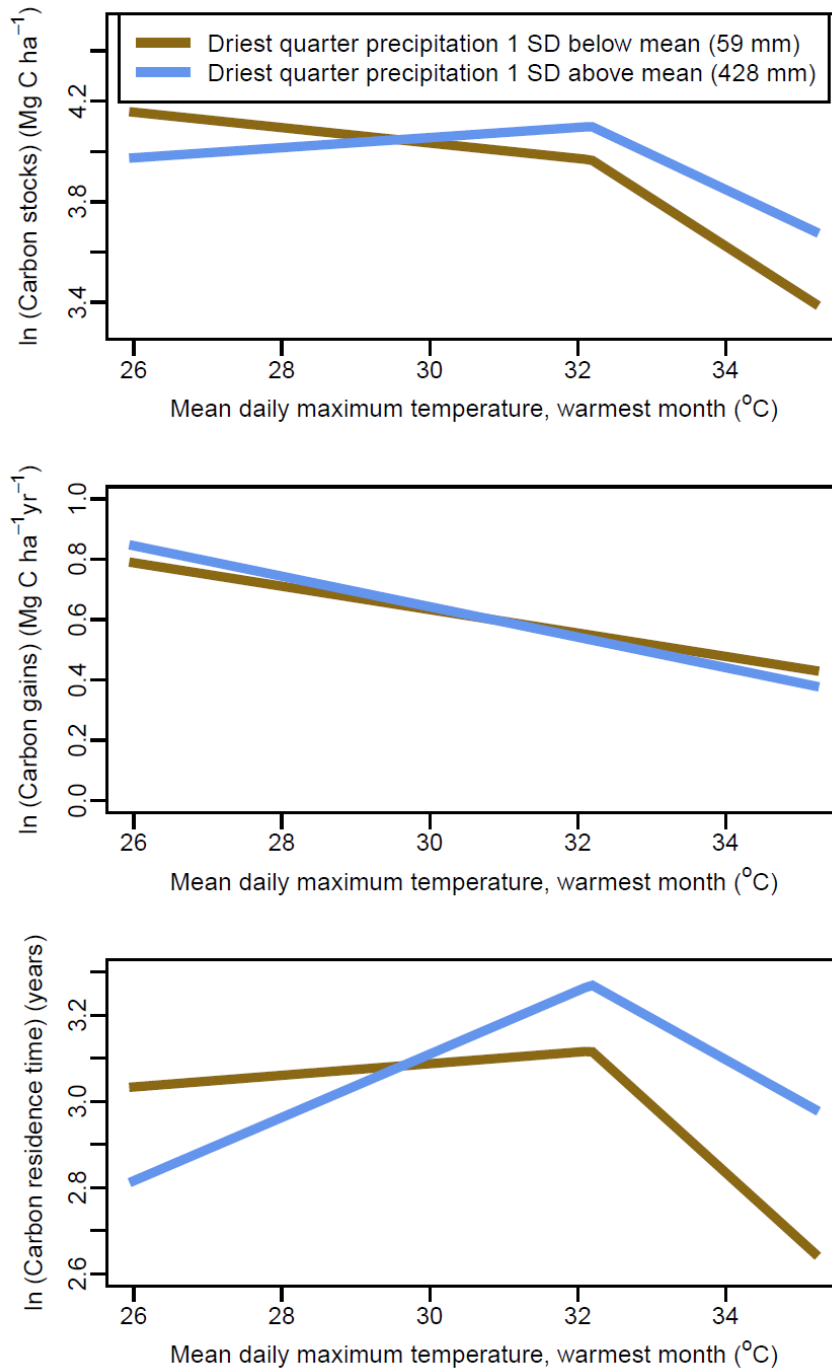
913

914 **Figure S5.** As Figure 2, but with aboveground biomass estimated using the Chave et al. 2005 (81)
915 moist forest allometric equation, which does not include a height term and is instead based on a third-
916 order polynomial relationship between diameter and aboveground biomass. This indicates that our
917 results are robust to using an alternative allometry to estimate aboveground biomass.

918

919

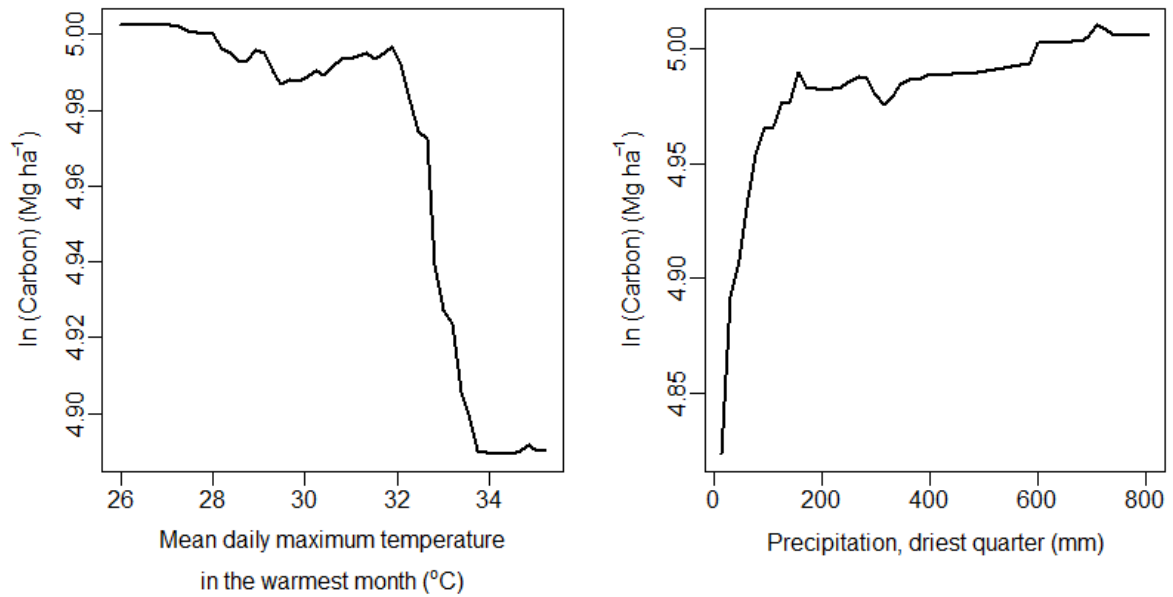
920



921

922 **Figure S6.** Interaction between mean daily maximum temperature in the warmest month and
 923 precipitation in the driest quarter in determining aboveground tropical forest carbon stocks, gains and
 924 residence time. Modelled relationships with temperature are shown holding precipitation either one
 925 standard deviation above or below the mean. Models with breakpoints are shown for carbon stocks
 926 and residence time as they were found to be better supported based on lower AIC ($\Delta AIC > 2$). Note
 927 that the temperature-carbon relationship is steeper when precipitation is low for carbon stocks and
 928 (above the breakpoint threshold) carbon residence time, but does not change with precipitation for
 929 carbon gains. Response curves are predicted with continent set as Africa.

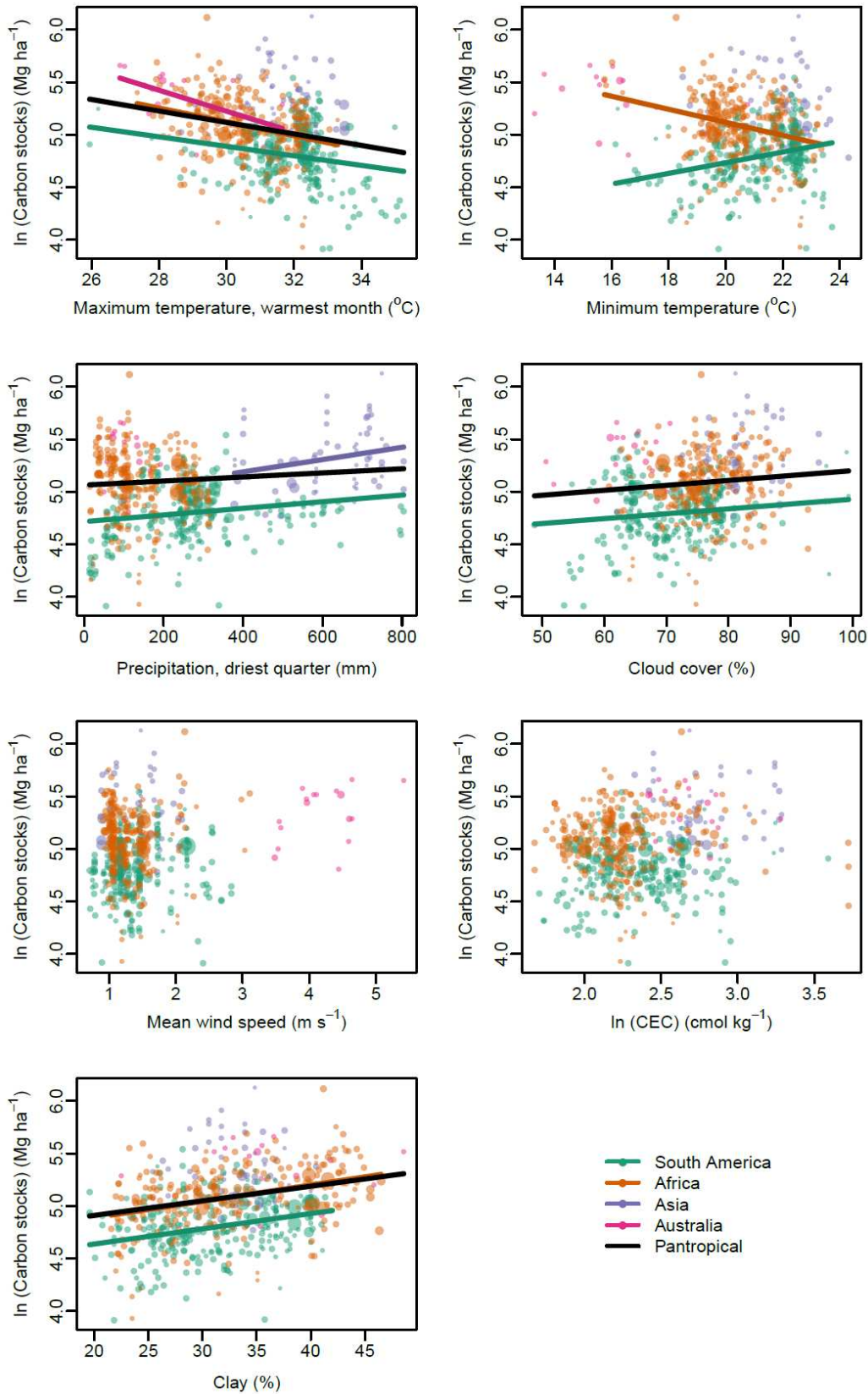
930



931

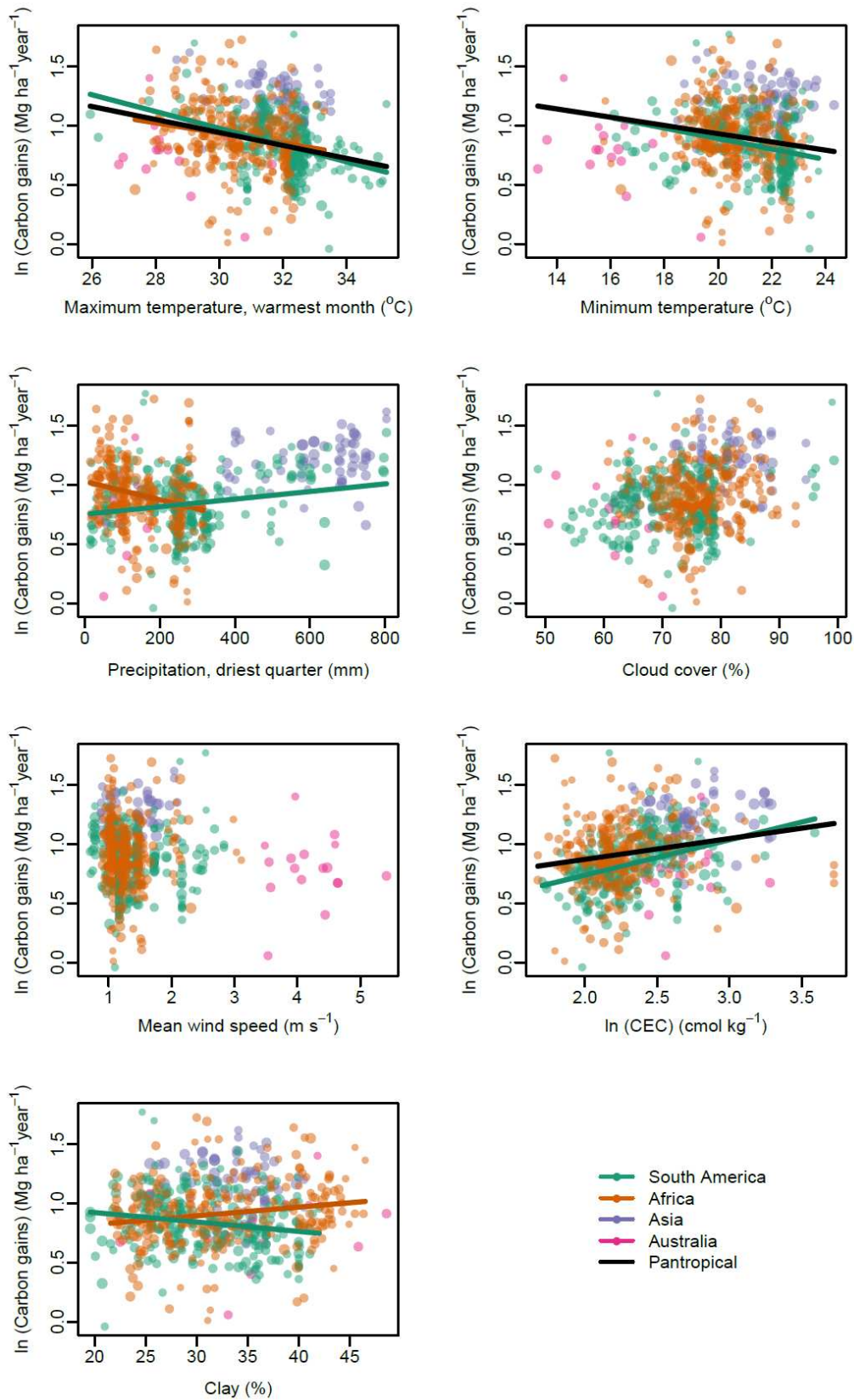
932 **Figure S7.** Partial relationships between tropical forest carbon stocks and the two climate variables
933 identified to be most important by the random forest decision tree algorithm. Partial plots show
934 predicted values of carbon stocks averaged across an ensemble of decision tree models when
935 changing the explanatory variable of interest and holding other variables constant. The importance of
936 variables in random forest analysis is assessed by calculating the average increase in node purity
937 across all decision trees (measured by residual sum of squares) when using the variable to split the
938 data. Higher values indicate greater importance. Maximum temperature increased node purity by 4.8
939 and precipitation by 4.7. For all other climate variables increases in node purity were < 3.5.

940



941

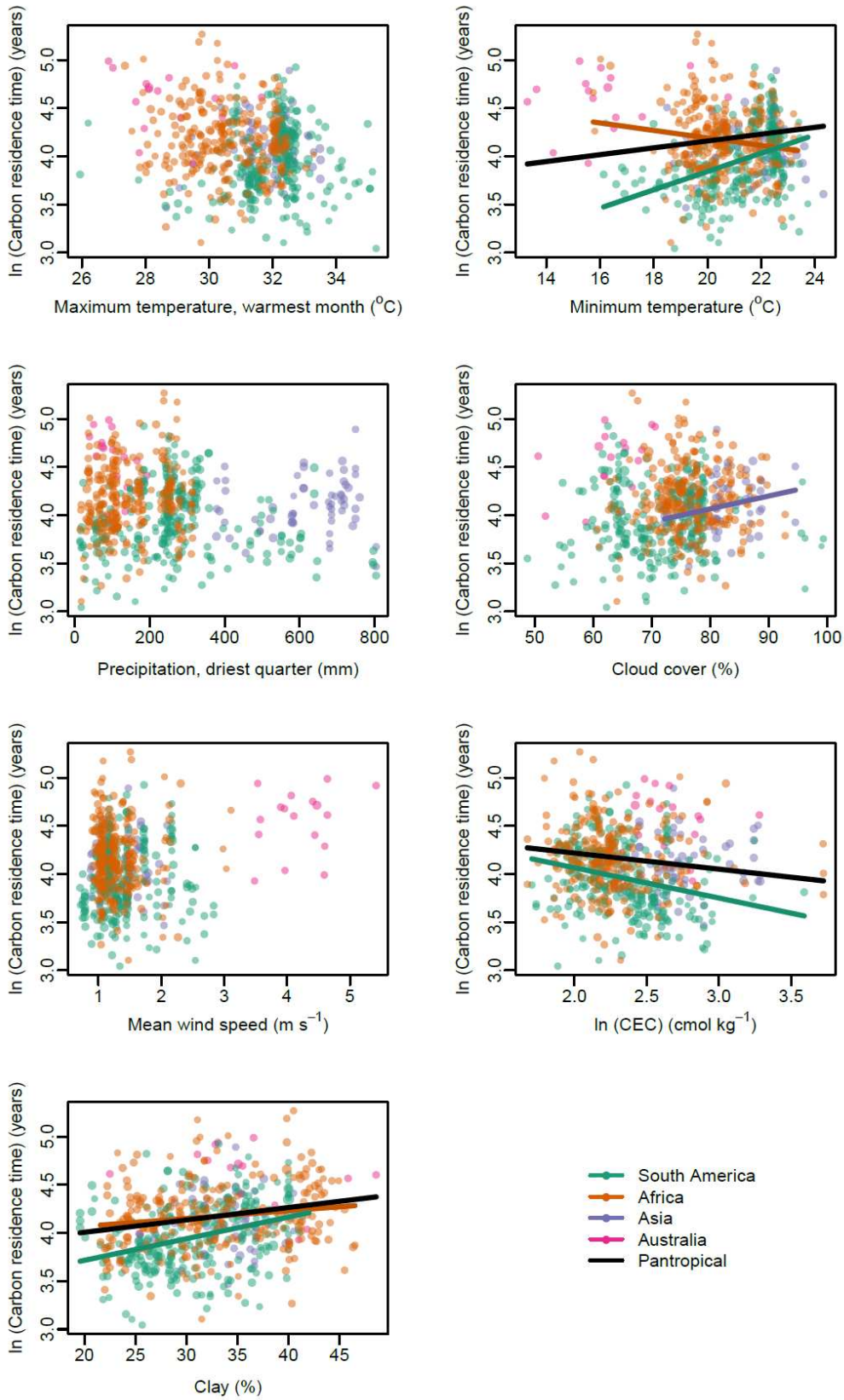
942 **Figure S8.** Relationships between aboveground tropical forest carbon stocks and environmental
 943 predictors. Symbols and colours as in Fig. 3. Coloured lines show bivariate relationships in each
 944 continent, and black lines show pan-tropical relationships also accounting for the effect of continent.
 945 Lines are only plotted where statistically significant.



946

947

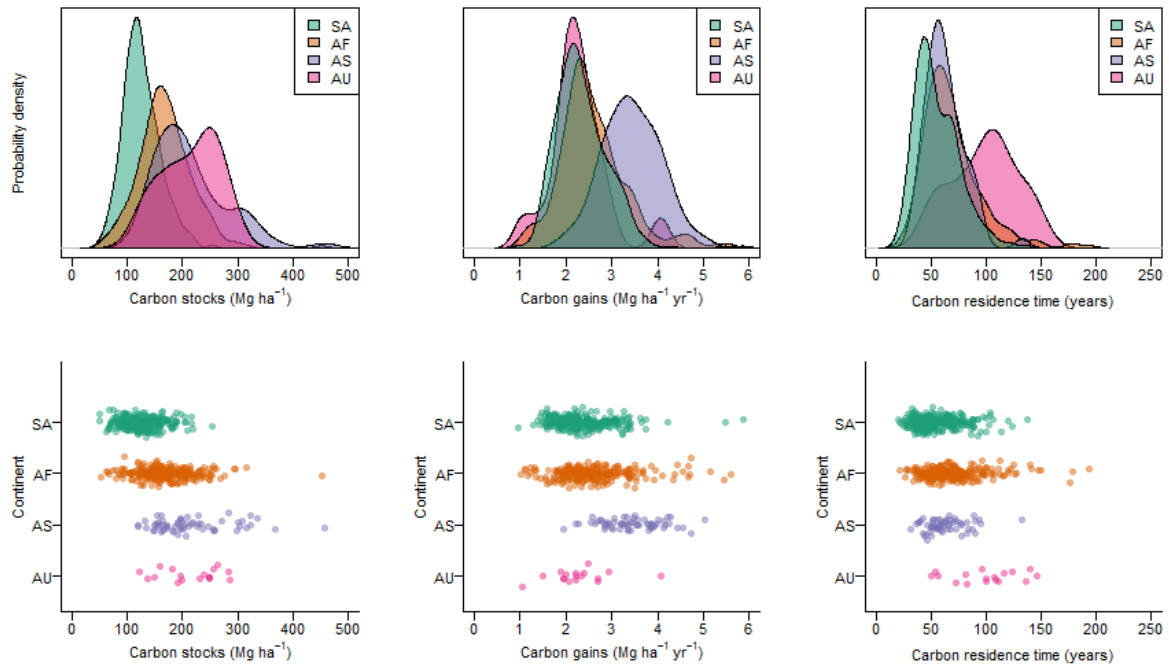
948 **Figure S9.** As Fig. S8, but showing relationships with carbon gains.



949

950 **Figure S10.** As Fig. S8, but showing relationships with carbon residence time.

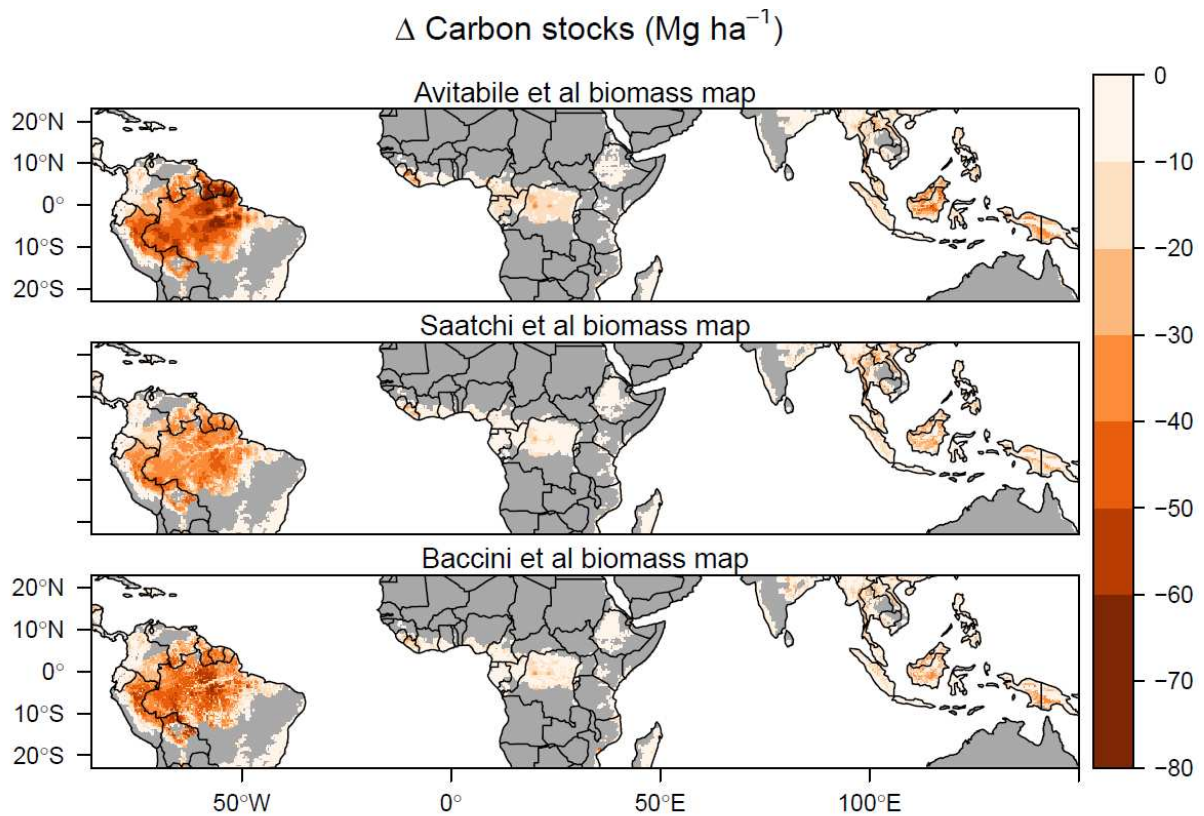
951



952

953 **Figure S11.** Variation in tropical forest aboveground carbon stocks, gains and residence time within
 954 and amongst continents. Data are presented as empirical probability density functions (top row) and
 955 dot-plots showing raw data points for all our multi-census plots (bottom row). SA = South America,
 956 AF = Africa, AS = Asia, AU = Australia.

957



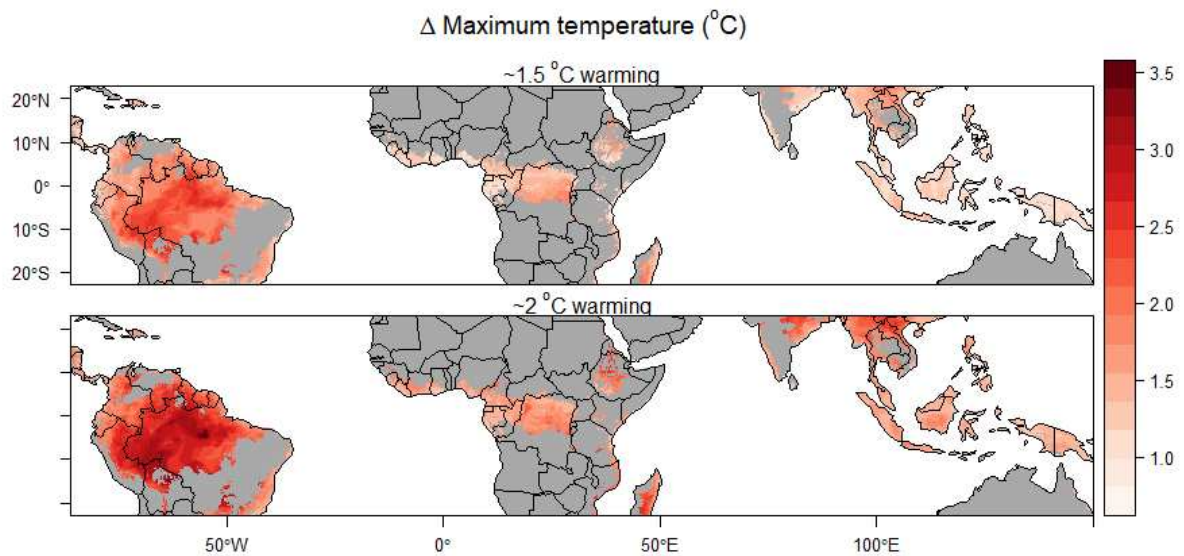
958

959 **Figure S12.** Effect of using earlier biomass reference maps for estimates of change in long-term
960 carbon stocks for global temperature increases of $\sim 2^\circ\text{C}$. Using aboveground biomass stock maps from
961 Saatchi et al. (64) and Baccini et al. (65) predicted biome-wide reductions in biomass carbon stocks
962 are 24.0 Pg (95 % CI = 5.8 – 39.6) and 28.4 Pg (95 % CI = 16.1 – 37.5) respectively. Under the \sim
963 1.5 $^\circ\text{C}$ warming scenario these are 18.4 Pg (5.8 – 30.5) and 21.1 Pg (10.2 – 29.4) respectively. Results
964 in the main text use the 2016 Avitabile et al. baseline map (30) – see methods for justification.

965

966

967



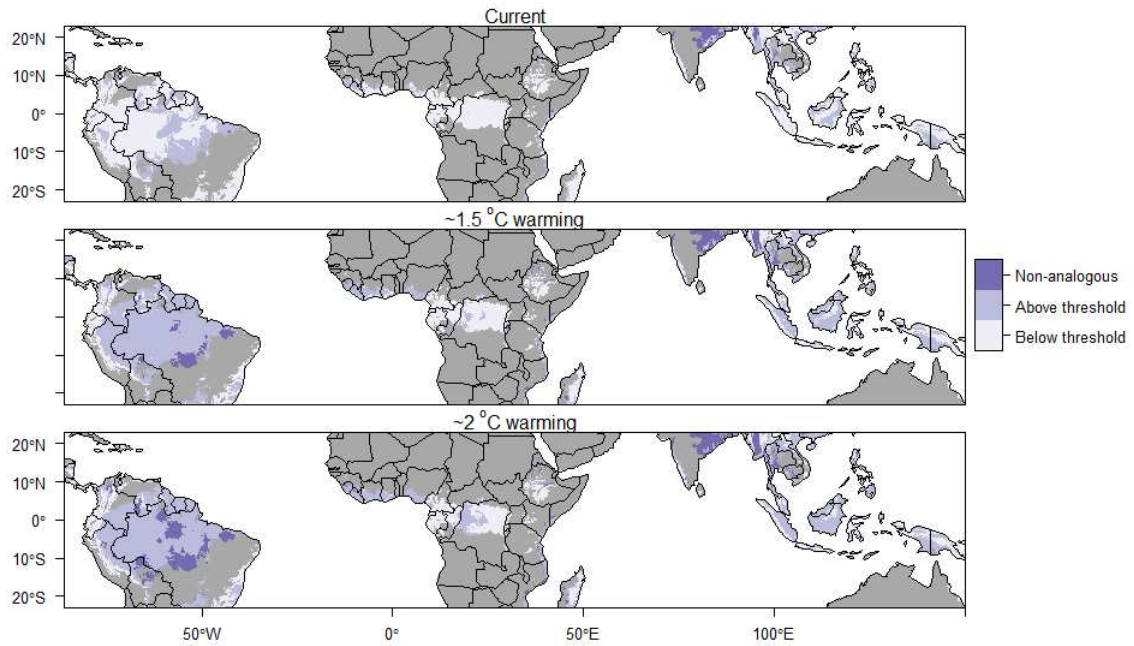
968

969 **Figure S13.** Biome-wide change in mean daily maximum temperature in the warmest month from
 970 present conditions (based on the Worldclim climatology, 1970-2000), given global increases in
 971 temperature of approximately 1.5 $^{\circ}\text{C}$ and 2 $^{\circ}\text{C}$ above pre-industrial levels. These levels of global
 972 temperature increase are obtained from, respectively, RCP 2.6, 2040-2060 and RCP 4.5, 2040-2060 to
 973 represent the potential spatial pattern of warming associated with global temperatures stabilising at
 974 these levels. Global temperature increases of 1.5 and 2 $^{\circ}\text{C}$ above pre-industrial levels (so ~0.8 $^{\circ}\text{C}$ and
 975 ~1.3 $^{\circ}\text{C}$ above our current baseline climate) would lead to mean increases in maximum temperature in
 976 the warmest month across the tropical forest biome of 1.9 $^{\circ}\text{C}$ and 2.4 $^{\circ}\text{C}$ the current baseline climate
 977 respectively.

978

979

980



981

982 **Figure S14** Areas of the biome above or below the 32.2°C threshold, above which carbon stocks
 983 decline more rapidly with temperature, under current conditions and two warming scenarios (see Fig.
 984 4). Areas warmer than any currently observed in our dataset (35.2°C) are also shown (non-analogous
 985 conditions). Note that even the 1.5°C warming scenario pushes most South American forests above
 986 the 32.2°C threshold.

987

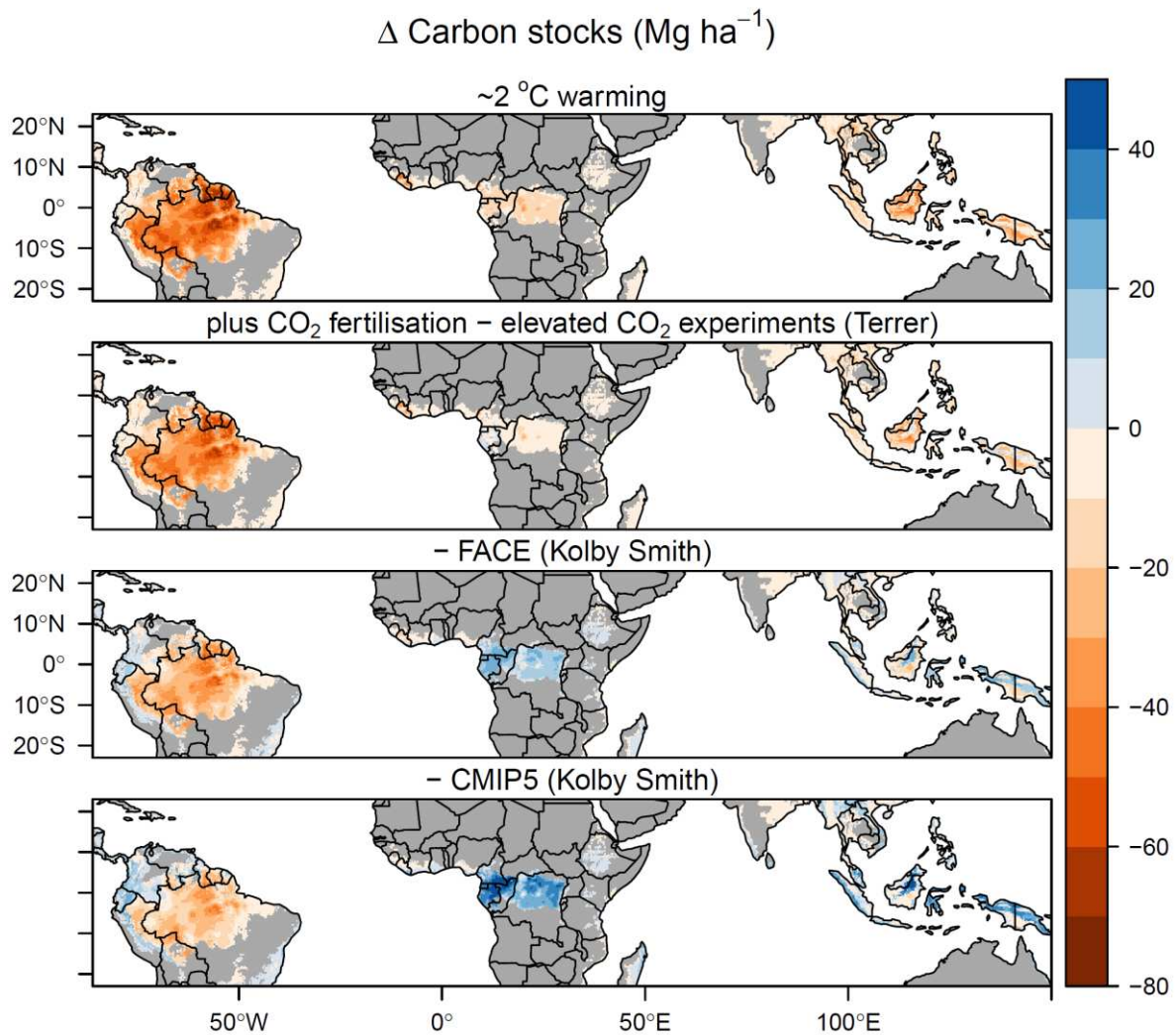
988

989

990

991

992



993

994 **Figure S15.** Predicted long-term change in aboveground carbon stocks under $\sim 2^\circ\text{C}$ global warming,
 995 based on either temperature effects alone or when also accounting for carbon dioxide growth
 996 stimulation. CO₂ fertilisation effects on equilibrium biomass levels were obtained from a recent
 997 synthesis of results of elevated CO₂ experiments (Terrer et al. (76)), free-air CO₂ enrichment (FACE)
 998 experiments (Kolby Smith et al. (73)) and CMIP5 earth system models (Kolby Smith et al. (73)).
 999 Depending on their strength, CO₂ effects either partially or fully ameliorate the biome-wide negative
 1000 effects of increasing temperatures on biomass carbon stocks (Table S3), but these carbon stocks are
 1001 predicted to decline over much of Amazonia even under the strongest CO₂ effect considered.

1002

1003

1004 **Table S1.** Climate variables selected for analysis and mechanisms by which they can affect carbon stocks.

| Climate property | Variable selected for analysis | Mechanism to affect carbon stocks |
|------------------------|---|--|
| Daytime temperature | Maximum temperature in the warmest month ¹ | High daytime temperatures exceed photosynthesis optima (82), increase evaporative stress, causing stomatal closure and reducing time for photosynthesis (26) and increase risk of mortality through hydraulic failure and/or carbon starvation (23). |
| Night-time temperature | Mean daily minimum temperature | Respiration rate increases with temperature so proportion of carbon taken through photosynthesis that is allocated to wood should decline with temperature (83). Increased respiration cost could also reduce tree longevity (23). As respiration occurs day and night, and photosynthesis only in the day, nighttime temperature should better reflect respiration effects and daytime temperature better reflect photosynthesis effects. |
| Moisture availability | Precipitation in the driest quarter ² | Moisture availability could limit photosynthesis and hence carbon gains, with stomata closing when moisture availability is limiting. The risk of mortality through hydraulic failure or carbon starvation is higher when moisture is limiting (23), and this could also set a limit on potential tree size and hence tree longevity. |
| Light availability | Cloud frequency | Increased photosynthesis and hence AGWP when light availability is greatest (i.e. cloud cover is low) (84). Alternatively, light availability could have a negative effect due to high evapotranspiration stress when cloud cover is low. |
| Wind speed | Mean wind speed | Carbon stocks are expected to be lower where physical damage through wind throw or breakage is higher, as carbon is removed more quickly from the system through mortality (85). But there is potential for greater carbon gains if forests are more dynamic. |

1005 ¹ Mean daily temperature in the warmest month (bio5) was selected instead of mean daily maximum temperature as it was more strongly decoupled from
1006 other climate variables. VPD could also represent some of these effects, but was too strongly correlation with maximum temperature to include as an
1007 independent variable.

1008 ² Moisture availability could also be represented by MCWD (maximum cumulative water deficit) or total precipitation, but only one of the three variables
1009 could be included in the model due to collinearity. MCWD was excluded as it is zero truncated, so less amenable to regression fitting.

1010

1011 **Table S2.** Coefficients of model-averaged general linear models of carbon stocks, gains and residence time as a function of climate, soil, continent and spatial
 1012 autocorrelation. Coefficients are AIC weighted averages across models with $\Delta AIC < 4$ from the best performing model; variables are given a score of zero if
 1013 they did not appear in a model. NA indicates that a term did not occur in any model in this set. MEM1-8 are spatial eigenvectors.

| Variable | Carbon stocks | | | | Carbon gains | | | | Carbon residence time | | | |
|------------------------------------|---------------|-------|-------|--------|--------------|-------|------|--------|-----------------------|-------|------|--------|
| | Estimate | SE | Z | P | Estimate | SE | Z | P | Estimate | SE | Z | P |
| Intercept - Africa | 4.986 | 0.010 | 476.9 | <0.001 | 0.571 | 0.525 | 1.09 | 0.278 | 3.909 | 0.688 | 5.67 | <0.001 |
| Minimum temperature | 0.031 | 0.019 | 1.67 | 0.096 | -0.001 | 0.007 | 0.18 | 0.861 | 0.019 | 0.022 | 0.88 | 0.381 |
| Maximum temperature, warmest month | -0.089 | 0.022 | 4.11 | <0.001 | -0.060 | 0.017 | 3.47 | <0.001 | -0.001 | 0.015 | 0.10 | 0.924 |
| Precipitation, driest quarter | 0.045 | 0.018 | 2.54 | 0.011 | -0.001 | 0.008 | 0.14 | 0.887 | 0.061 | 0.023 | 2.70 | 0.007 |
| Cloud frequency | 0.002 | 0.008 | 0.24 | 0.814 | -0.006 | 0.011 | 0.54 | 0.592 | 0.025 | 0.021 | 1.17 | 0.241 |
| Wind speed | 0.004 | 0.012 | 0.38 | 0.705 | 0.016 | 0.020 | 0.78 | 0.437 | -0.004 | 0.015 | 0.24 | 0.807 |
| Soil texture (% clay) | 0.021 | 0.017 | 1.26 | 0.208 | -0.005 | 0.011 | 0.49 | 0.628 | 0.040 | 0.018 | 2.17 | 0.030 |
| Soil fertility (CEC) | -0.003 | 0.009 | 0.34 | 0.732 | 0.005 | 0.011 | 0.51 | 0.613 | -0.012 | 0.017 | 0.70 | 0.486 |
| MEM1 | 0.115 | 0.014 | 7.96 | <0.001 | 0.319 | 0.559 | 0.57 | 0.569 | 0.375 | 0.734 | 0.51 | 0.610 |
| MEM2 | 0.098 | 0.017 | 5.67 | <0.001 | 0.083 | 0.273 | 0.30 | 0.762 | 0.286 | 0.359 | 0.80 | 0.427 |
| MEM3 | -0.025 | 0.014 | 1.84 | 0.065 | 0.014 | 0.041 | 0.34 | 0.735 | 0.007 | 0.054 | 0.12 | 0.904 |
| MEM4 | -0.021 | 0.011 | 1.84 | 0.066 | -0.038 | 0.020 | 1.84 | 0.066 | -0.002 | 0.027 | 0.07 | 0.945 |
| MEM5 | 0.027 | 0.011 | 2.46 | 0.014 | 0.020 | 0.015 | 1.33 | 0.182 | 0.020 | 0.020 | 0.98 | 0.327 |
| MEM6 | 0.017 | 0.011 | 1.56 | 0.118 | 0.025 | 0.011 | 2.34 | 0.019 | -0.014 | 0.014 | 1.05 | 0.293 |
| MEM7 | 0.010 | 0.011 | 0.93 | 0.353 | -0.017 | 0.010 | 1.61 | 0.107 | 0.036 | 0.014 | 2.57 | 0.010 |
| MEM8 | -0.072 | 0.013 | 5.64 | <0.001 | 0.057 | 0.012 | 4.91 | <0.001 | -0.127 | 0.016 | 7.80 | 0.000 |
| Asia | NA | | | | 0.380 | 0.542 | 0.70 | 0.485 | -0.753 | 0.683 | 1.10 | 0.271 |
| Australia | NA | | | | -0.173 | 0.390 | 0.44 | 0.658 | 0.006 | 0.516 | 0.01 | 0.990 |
| South America | NA | | | | 0.643 | 1.164 | 0.55 | 0.582 | 0.542 | 1.530 | 0.35 | 0.724 |

1015 **Table S3.** Predicted biome-wide changes in long-term biomass carbon stocks (scaled to include root
 1016 biomass) under global temperature increases of $\sim 1.5^{\circ}\text{C}$ and $\sim 2^{\circ}\text{C}$. Changes are based on temperature
 1017 effects alone, and when also accounting for the effect of increased CO_2 concentrations on tree growth.
 1018 CO_2 effects were obtained from a synthesis of results of elevated CO_2 experiments (Terrer et al. (76)),
 1019 free-air CO_2 enrichment (FACE) experiments (Kolby Smith et al. (73)) and CMIP5 earth system
 1020 models (Kolby Smith et al. (73)). 95% confidence intervals around changes (based on uncertainties in
 1021 temperature effects alone) are shown in parentheses.

| CO ₂ effect | Change in biomass carbon stocks (Pg) | |
|---|--|--|
| | $\sim 1.5^{\circ}\text{C}$ warming (443 ppm CO ₂) | $\sim 2^{\circ}\text{C}$ warming (487 ppm CO ₂) |
| None | -26.9 (-38.4 - -15.8) | -35.3 (-49.0 - -20.9) |
| Terrer et al. elevated CO ₂ experiments | -22.0 (-33.0 - -9.9) | -26.3 (-37.6 - -11.5) |
| Kolby Smith et al. FACE experiments | -6.2 (-16.8 - 7.7) | -9.9 (-24.3 - 3.9) |
| Kolby Smith et al. CMIP5 models | 3.9 (-8.3 - 12.6) | 2.0 (-11.9 - 19.8) |

1022